Innate Behavior Sequence Progression by Peptide-Mediated Interorgan Crosstalk

Fabiana Heredia[1,*], Yanel Volonté[1,2,*], Joana Pereirinha[1,‡,*], Magdalena Fernandez-Acosta[1], Andreia P. Casimiro[1], Cláudia G. Belém[1‡‡], Filipe Viegas§[1], Kohtaro Tanaka[4,¶], Maite Arana[2], Gisele A. Cardoso[1,3,#], André Macedo[1], Malwina Kotowicz[1,**], Facundo H. Prado Spalm[2], Marcos J. Dibo[2], Raquel D. Monfardini[1,3], Tatiana T. Torres[3], César S. Mendes[1], Andres Garelli[1,2,†], Alisson M. Gontijo[1,†]

[1] CEDOC, Chronic Diseases Research Center, NOVA Medical School | Faculdade de Ciências Médicas, Universidade Nova de Lisboa, Lisbon, Portugal

[2] INIBIBB, Instituto de Investigaciones Bioquímicas de Bahia Blanca, Universidad Nacional del Sur - CONICET, Argentina.

[3] Laboratório de Genômica e Evolução de Artrópodes, Departamento de Genética e Biologia Evolutiva, Universidade de São Paulo - São Paulo, Brazil.

[4] Instituto Gulbenkian de Ciências, Oeiras, Portugal.

* These authors contributed equally to this work

† Corresponding authors: agarelli@inibibb-conicet.gob.ar (A.G.) and alisson.gontijo@nms.unl.pt (A.M.G.)

‡ Present address: Institute of Molecular Biology, Mainz, Germany.

‡‡ Present address: The Francis Crick Institute, London, UK.

§ Present address: Department of Molecular Life Sciences, University of Zurich, Zurich, Switzerland.

¶ Present address: Fred Hutchinson Cancer Research Center, Seattle, U.S.A.

Present address: CBMEG, Universidade Estadual de Campinas, Campinas, Brazil.

** Present address: DZNE, Helmholtz Association, Bonn, Germany.

Innate behaviors consist of a succession of genetically-hardwired motor and physiological subprograms that can be coupled to drastic morphogenetic changes. How these integrative responses are orchestrated is not completely understood. Here, we provide insight into these mechanisms by studying pupariation, a multi-step innate behavior of fly larvae that is critical for survival during metamorphosis. We find that the steroid-hormone ecdysone triggers parallel pupariation neuromotor and morphogenetic subprograms, which include the induction of the relaxin-peptide hormone, Dilp8, in the epidermis. Dilp8 acts on six Lgr3-positive thoracic interneurons to couple both subprograms in time and to instruct neuromotor subprogram switching during behavior. Our work reveals that interorgan feedback gates progression between subunits of an innate behavior and points to an ancestral neuromodulatory function of relaxin signaling.

Innate (*i.e.,* intrinsic) behaviors are genetically-hardwired behaviors that do not require previous learning or experience for proper execution[1, 2]. These behaviors comprise neuromotor and physiological subprograms that are many times coupled to drastic morphogenetic changes. For instance, males of some pacific salmonid species undergo dramatic morphological changes during spawning migration[3], and females of many mammalian species remodel their pubic ligaments to favor delivery during parturition behavior[4-6]. Holometabolan insects, those with complete metamorphosis, have evolved different innate behaviors and processes that promote survival during this critical life-history stage[7-9]. Honey bees, for instance, metamorphose within wax-sealed hive-chambers, while some lepidopterans (butterflies and moths) pupate within spun cocoons. Cyclorraphous flies, such as *Drosophila*, undergo metamorphosis within a puparium, a protective capsule consisting of the reshaped and hardened ecdysed cuticle of the last larval instar[7, 8, 10].

Puparium formation (pupariation) is associated with additional survival-promoting behaviors, including the extrusion of anterior spiracles for efficient gas exchange, and the expulsion and spreading of a salivary-gland-derived secretory "glue" that attaches the puparium to its substrate[11-14]. Proper pupariation therefore requires tight coordination between associated behavioral subprograms, body-reshaping motor subprograms, and non-motor morphogenetic processes, such as the cuticle sclerotization subprogram that fixes the achieved

morphological changes of the puparium[7, 10, 15]. Although the whole pupariation process is known to be triggered by a surge in the levels of the steroid hormone 20-hydroxyecdysone (20HE) at the end of the third instar larval phase[7, 16-18], the downstream programs are thought to be mediated by specific neuroendocrine signals and circuits, most of which remain to be characterized[7, 19-22]. Furthermore, how subprograms of innate behaviors are coordinated amongst themselves and in time is not fully understood.

The Dilp8-Lgr3 pathway is required for puparium morphogenesis

During the first half of the last larval instar, an imaginal disc growth checkpoint system mediated by the disc-derived stress signal, the relaxin-like peptide hormone *Drosophila* insulin-like peptide 8 (Dilp8)[23, 24], and its neuronal receptor, the Leucine Rich Repeat containing G protein coupled receptor 3 (Lgr3)[25-28], contributes to the development of proportionate adult body parts by transiently antagonizing 20HE biosynthesis by the prothoracic gland[23-46]. Here, we serendipitously found that mutation (*Lgr3*^{ag1})[26, 47] or ubiquitous RNA interference (RNAi)-mediated knockdown of *Lgr3* using the GAL4-UAS system (*UAS-Lgr3-IR*)[26], generates aberrantly shaped puparia that are slightly thinner and more elongated than their wild-type (WT) background controls, as measured by puparium aspect ratio (AR = length/width) (Fig. 1A-D). Less penetrant phenotypes include defective retraction of the anteriormost pre-spiracular segments into the body (anterior retraction) and failure to extrude the anterior spiracles. Similar phenotypes were observed in five *dilp8* loss-of-function mutants generated here by CRISPR/Cas9-mediated directed mutagenesis[48, 49] (Fig. 1E, F, Extended Data Fig. 1A) (see also Methods and Extended Data Fig. 1B-E), and in an independent knock-out allele *dilp8*^{KO} [40] (Extended Data Fig. 1F, G). These findings suggested that animals lacking Dilp8-Lgr3 signaling have problems contracting their body into the puparium shape and/or stabilizing their remodeled body at the contracted state.

Lgr3 is required in a new subset of neurons for proper puparium morphogenesis

To ask in which tissue *Lgr3* is required for puparium morphogenesis control, we carried out tissue-specific *Lgr3* RNAi knockdown. Puparium AR was most strongly increased when *Lgr3* was knocked-down in neurons using the pan-neuronal synaptobrevin promoter-fusion GAL4 line, *R57C10-GAL4* (*R57C10>*)[50, 51] (Fig. 1G). As *Lgr3* is also required in neurons for imaginal disc growth coordination before the midthird instar transition (MIT)[23-28, 34, 46] (Fig.

1H-I), this finding poses the question if the puparium morphogenesis defect of *dilp8* and *Lgr3* mutants arises from the abrogation of this same early signaling event.

Fig. 1.

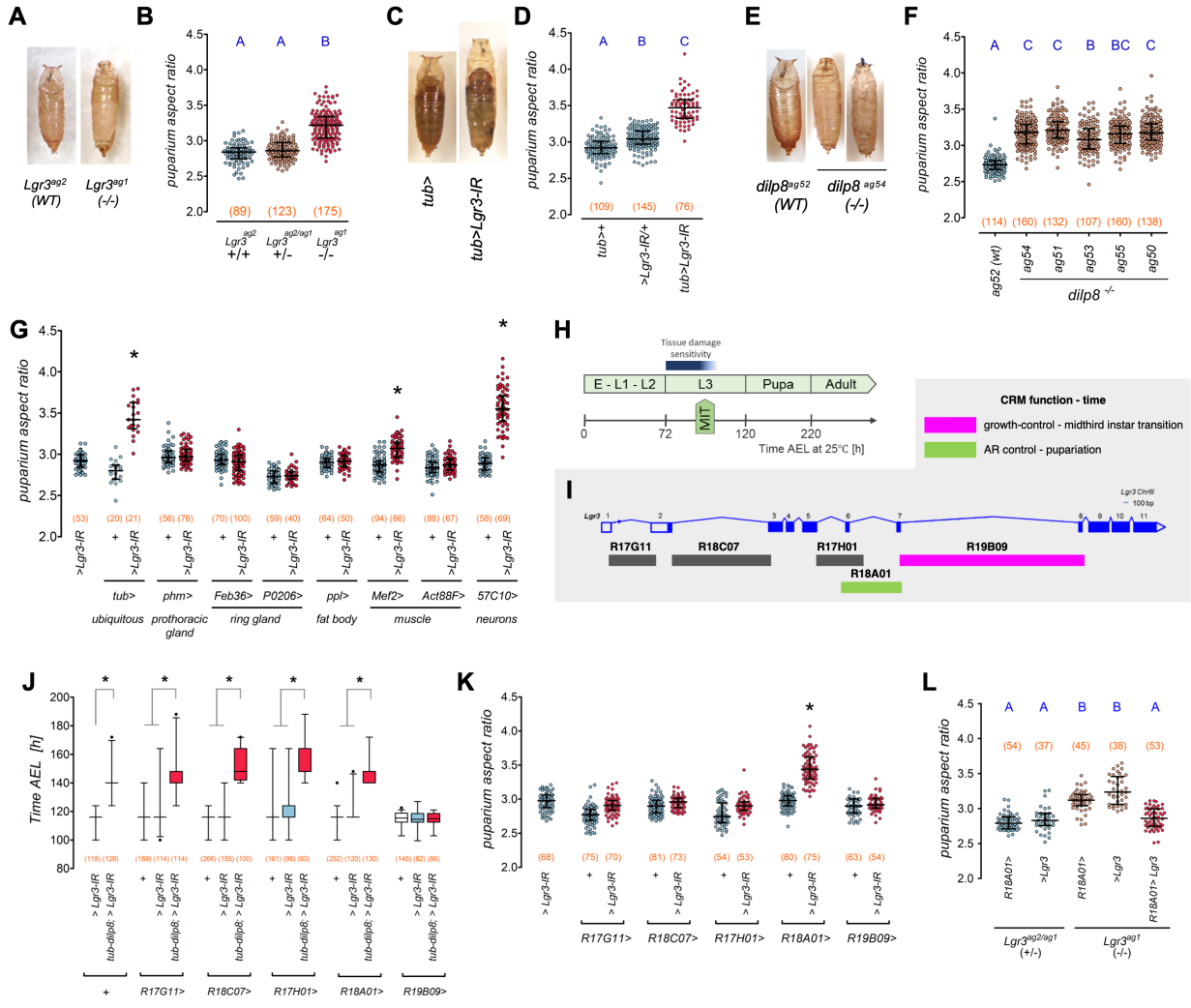

Fig. 1: Puparium morphogenesis requires Dilp8-Lgr3 signaling in neurons

A,C,E. Representative photos of puparia from the depicted genotypes. **B,D,F,G,K,L.** Dot plots of puparium aspect ratio (AR). Dots: one animal. **B.** *Lgr3* mutation increases puparium AR. **D.** *tub>Lgr3-IR* increases puparium AR. **F.** *dilp8* mutation increases puparium AR. **G.** Pan-neuronal *Lgr3* knockdown (*57C10>*) increases puparium AR similarly to ubiquitous knockdown (*tub>*). **H.** Sensitivity to tissue-damage-induced Dilp8 occurs before the midthird instar transition (MIT). Time after egg laying (AEL) in h. **I.** *Lgr3* locus scheme with its Cis-Regulatory Motifs (CRM) and known activities. **J.** *tub-dilp8*-induced developmental delay rescue by *R19B09>Lgr3-IR*. Box plots showing

pupariation time. **K.** Knockdown of *Lgr3* in R18A01, but not in R19B09 neurons, increases the puparium AR. **L.** Rescue of the puparium AR defect of $Lgr3^{ag1}$ mutants by *R18A01>Lgr3.* Statistics: **B,D,F,G,K,L.** Horizontal bar, median. Error bars: 25-75% percentiles. **J.** Whiskers, 5-95%. Dots, outliers. **B,D,F,L.** Same blue letter, $P>0.05$. **B,D,F,L.** Dunn's test. **G,J,K.** Dunn's test, compared to both *>Lgr3-IR* and respective *GAL4>+* control. (N) Number of animals (red). *$P<0.05$.

Imaginal disc-derived Dilp8 acts on a subpopulation of *Lgr3*-positive CNS neurons that can be genetically manipulated using the cis-regulatory module (CRM) *R19B09* [25-28, 50, 52, 53] (Fig. 1H-I). Accordingly, RNAi knockdown of *Lgr3* using *R19B09-GAL4* (*R19B09>Lgr3-IR*), but not four other *Lgr3* CRM GAL4 lines tested (Fig. 1I), specifically suppresses the developmental delay caused by *dilp8* overexpression under the direct control of the *tub* [*tub-dilp8*, Ref.[27]] (Fig. 1J). However, *R19B09>Lgr3-IR* had no effect on puparium AR (Fig. 1K). Of the four other CRM-GAL4 lines tested, only *R18A01-GAL4* (*R18A01>*) strongly increased puparium AR when driving *Lgr3-IR* (Fig. 1I and 1K). These results clearly show that proper puparium morphogenesis does not require Lgr3 in the growth-coordinating R19B09 neurons. Instead, Lgr3 is required in a new population of cells that can be genetically manipulated using the *R18A01>* driver. Consistent with this, the puparium morphogenesis defect of $Lgr3^{ag1}$ mutants could be completely rescued by expressing an *Lgr3* cDNA [*UAS-Lgr3*; Ref.[26]] under the control of *R18A01>* (Fig. 1L). We conclude that the control of the onset of metamorphosis and the control of puparium morphogenesis are two independent processes that require *Lgr3* in two separate populations of neurons marked by *R19B09>* and *R18A01>*, respectively (Fig. 1I).

20HE signaling induces dilp8 transcription in the cuticle epidermis during pupariation

We next investigated the source of the Dilp8 signal that controlled puparium morphogenesis. A series of genomewide transcriptional studies indicated that *dilp8* transcripts are strongly upregulated in the carcass, a tissue composed majorly of cuticle epidermis and muscle, and to a lesser extent of sessile hemocytes, neurons, and other cell types, at the onset of pupariation [white prepupae (WPP T0)], and in an ecdysone-receptor-dependent manner[46, 54-56] (Extended Data Fig. 2A-C). We confirmed and expanded these data using quantitative reverse-transcriptase polymerase chain reaction (qRT-PCR) with cDNA obtained from whole

synchronized larvae or their dissected tissues (see Methods). We find that *dilp8* mRNA levels increase three orders of magnitude between post-feeding 3rd instar larvae (*i.e.,* "wandering" stage) and early pupariating animals, and a decrease in the peak can be detected as soon as 1.0 h after WPP T0 ("T30", Fig. 2A). The WPP T0 upregulation is largely explained by a strong increase in carcass-derived *dilp8* mRNA (Fig. 2B). These results suggest that the upregulation of *dilp8* mRNA in the carcass at pupariation is part of the normal developmentally-triggered 20HE-dependent pupariation process[17].

Fig. 2.

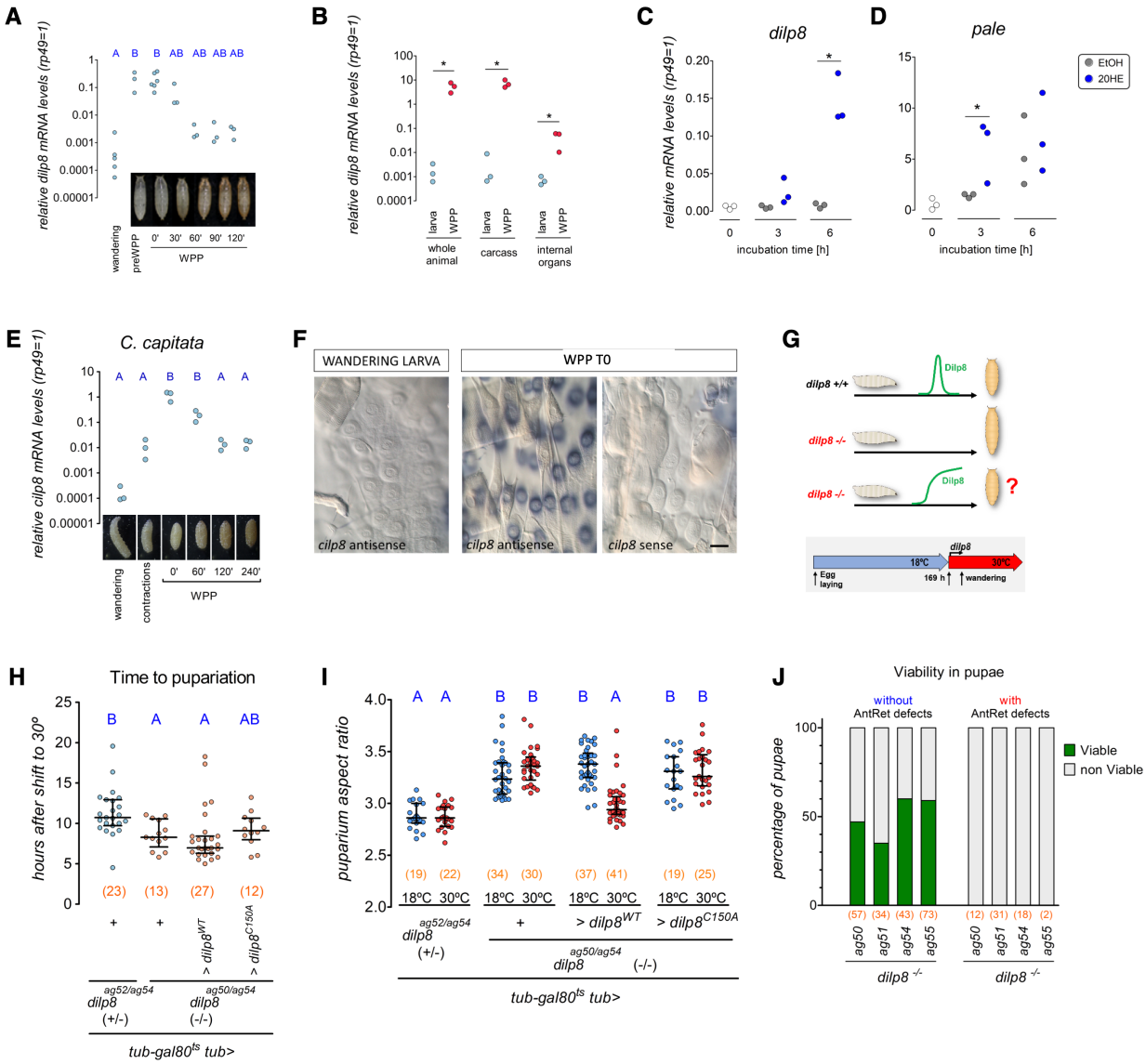

Fig. 2: A conserved *dilp8* expression peak in the cuticle epidermis is required for puparium morphogenesis and viability.

A-E,H,I. Dot plots showing **A-C.** qRT-PCR estimations of *dilp8*, **D.** *pale,* and **E.** *C. capitata ilp8* (*cilp8*) mRNA levels (Dots: biological repeats), **H.** time to pupariation, and **I.** pupariation aspect ratio (AR). **A.** *dilp8* and **E.** *cilp8* are transiently expressed at white-prepupa WPP T0. **B.** *dilp8* transcripts are enriched in the WPP carcass. **C.** *dilp8* and **D.** *pale* mRNA levels in carcasses treated with 20HE or etOH *in vitro*. **F.** *in situ* hybridization with *cilp8* antisense probe stains epidermal cells on *C. capitata* WPP T0 carcasses. **G.** *dilp8* rescue scheme used in **H,I. H.** *dilp8* expression after the MIT (*tub>dilp8*^{WT} at 30°C) does not delay pupariation time, but **I.** rescues the puparium AR of *dilp8* mutants. **J.** Percentage of viable pupae (green) with and without anterior retraction (AntRet) defects. Failure in AntRet decreases pupal viability. Statistics: **H,I.** Horizontal bar, median. Error bars: 25-75% percentiles. **A,E,H,I.** Same blue letter, $P>0.05$. **A,H,I.** Dunn's test. **E.** Student-Newman-Keuls test. **B-D.** Student's t-test. *$P<0.05$**.** (N) Number of animals (red). Scale bar, 50 µm.

However, as the whole pupariation program is dependent on 20HE signaling, which peaks -4 h before pupariation[17, 55], it is not clear whether or not this is a consequence of direct action of 20HE on the carcass. To test this, we incubated dissected carcasses from 3rd instar larvae collected at 96 h after egg laying with 20HE for 3 or 6 h and assayed for *dilp8* mRNA levels by qRT-PCR. As expected, *dilp8* mRNA was upregulated by a factor of 30.0 at 6 h and was not affected by ethanol vehicle treatment (Fig. 2C), indicating that *dilp8* is a direct target of 20HE-dependent signaling in the carcass. The *dilp8* expression pattern was nevertheless different from another 20HE-dependent epidermis-transcribed gene, *pale* (*ple, Tyrosine 3-monooxygenase*)[55, 56] (Extended Data Fig. 2D-F)). While 20HE also slightly stimulated *pale* mRNA levels, the carcass cells obtained 96 h after egg laying were clearly already committed to increase *pale* mRNA levels, independently of further 20HE exposure (Fig. 2D). This is consistent with previous reports that show *pale* mRNA levels already upregulated at -4 h before pupariation, whereas *dilp8* mRNA levels remain at basal level[56] (Extended Data Fig. 2A, D)). These results suggest that *dilp8* is a direct target of very late 20HE-dependent signaling, probably the strongest and last peak preceding pupariation (at -4 h), whereas *pale* is induced by smaller and earlier 20HE peaks, probably the MIT peak[18, 34]. This 20HE activity upstream of *dilp8* during pupariation is the opposite of what occurs in early 3rd instar larvae, when Dilp8 originating from abnormally-growing imaginal discs acts upstream of 20HE, inhibiting its biosynthesis[23-28, 34, 46].

The ilp8 transcriptional peak at pupariation is conserved in a distant cyclorrhaphan

We next asked if this *ilp8* peak at pupariation is conserved in other puparium-forming insects. For this, we characterized the pupariation program of the Tephritidae fly *Ceratitis capitata* (Fig. 2E; see Methods). We extracted mRNA from animals synchronized at specific stages of pupariation, and quantified the *Ceratitis insulin-like peptide 8* ortholog (*cilp8*) mRNA levels using qRT-PCR and the *Ceratitis rp49* ortholog as a control gene. Our results show a very strong, up to four-orders of magnitude, upregulation of *cilp8* mRNA levels at WPP "T0" (Fig. 2E). Interestingly, the levels of *cilp8* mRNA were already upregulated by a factor of ~88 at the ~5-min "body contraction" phase that precedes early WPP formation by 1-1.5 h (Fig. 2E), suggesting that *cilp8* can act very early or before the pupariation behavior begins. The levels at 2 h after T0 (T120) were still ~100-fold higher than wandering stage larvae (Fig. 2E), indicating that the *cilp8* peak might be broader in *C. capitata* than in *D. melanogaster.* Nevertheless, these results indicate that the upregulation of *ilp8* at the time of puparium formation has been conserved for at least the time since *Drosophila* and *Ceratitis* shared their last common ancestor approximately 126 million years ago (MYA) [confidence interval (97-153 MYA)][57].

To pinpoint the source of *cilp8* upregulation in the carcass of WPP T0 animals, we carried out *in situ* hybridization using a *cilp8* antisense probe. Strong staining was detected in epidermal cells of the cuticle of WPP T0 animals (Fig. 2F). Consistently, no signal was detectable in post-feeding 3rd instar larvae or in WPP T0 animals probed with a control sense *cilp8* probe (Fig. 2F). These results corroborate the findings in *Drosophila,* strongly suggesting that a conserved surge of *ilp8* occurs in the cuticle epidermis downstream of the 20HE signaling event that instructs the animal to initiate the pupariation program.

Dilp8 is required during pupariation for proper puparium morphogenesis

To genetically test if the pupariation-associated *dilp8*-mRNA peak is the primary source of Dilp8 activity that signals to Lgr3 in *R18A01* neurons to mediate proper puparium morphogenesis, we hypothesized that ectopic expression of a *dilp8* cDNA after the MIT checkpoint, a timepoint after which animals are no longer sensitive to the tissue damage-stress signal[34] (Fig. 1H), could rescue the increased AR phenotype of *dilp8* mutants (Fig. 2G).

To control *dilp8* expression temporally, we placed a GAL4-dependent *dilp8* expression system (*tub>dilp8*) together with a ubiquitously-expressed temperature-sensitive GAL4-inhibitor, *tub-GAL80ts*, carried out a temperature switch after the MIT, and scored the timing of pupariation and puparium AR. As expected, the activation of *tub>dilp8* after the MIT did not delay the onset of metamorphosis (Fig. 2H), confirming that at this timepoint Dilp8 is no longer able to signal via *R19B09>*-positive neurons to inhibit ecdysone biosynthesis and delay the onset of metamorphosis. However, activation of *tub>dilp8* after the MIT was sufficient to completely rescue the increased puparium AR of *dilp8* mutants (Fig. 2I). In contrast, activation of a mutant *dilp8* cDNA $dilp8^{C150A}$, which carries no Dilp8 activity due to the substitution of a critical cysteine to alanine[24], had no effect on puparium AR. These results are in line with the independence of the puparium AR phenotype on the *R19B09>*-positive neurons. Our attempts to genetically knockdown or knockout *dilp8* specifically in cells of the cuticle epidermis to substantiate this finding were unsuccessful due to technical limitations (namely *dilp8* RNAi inefficiency and epistatic epidermal phenotypes caused by Cas9 expression, see Methods and Extended Data Fig. 1B-E, Extended Data Fig. 2G, H). Nevertheless, taking together the spatial and temporal expression and rescue data, our results are strongly consistent with a model where the pupariation-associated upregulation of *dilp8* mRNA in the cuticle epidermis is the source of the Dilp8 peptide that signals via Lgr3 in *R18A01>*-positive neurons in the CNS.

Proper anterior retraction requires the Dilp8-Lgr3 pathway and is essential for development

While the puparium shape defect of *dilp8* and *Lgr3* mutants is evident at the population level, the phenotype follows a normal distribution and includes animals with puparium ARs overlapping the normal spectrum (*e.g.,* see Fig. 1B, F). Likewise, failure to retract anterior segments is also incompletely penetrant, occurring in 5-40% animals, depending on the *dilp8* allele (Extended Data Fig. 2I, J). *dilp8* and *Lgr3* mutants also show incomplete pupal viability (Extended Data Fig. 2K). Similar results were obtained by ubiquitous or panneuronal RNAi knockdown of *Lgr3* (*tub>Lgr3-IR* or *R57C10>Lgr3-IR*, respectively) confirming that the phenotype is specific for loss of *Lgr3* activity in neurons (Extended Data Fig. 2L). To test if this lethality was due to anterior retraction defects, we followed pupal viability in animals with gross anterior retraction defects. We find that 100% of animals with visible anterior retraction defects fail to eclose, suggesting that proper anterior retraction is critical for pupal viability (Fig. 2H). Nevertheless, the fact that a fraction of mutants achieves

WT-level puparium AR and at least something that looks like proper anterior retraction of the pre-spiracular segments proves that the Dilp8-Lgr3 pathway is not *per se* the signal for anterior retraction. Rather, this suggests that the role played by Dilp8-Lgr3 in anterior retraction and proper puparium AR remodeling is modulatory and the mechanism might involve the regulation of a thresholded system. To learn more about the mechanism underlying the pupariation-specific defects of Dilp8-Lgr3 pathway mutants, we decided to observe pupariation directly.

Direct observation of pupariation motor program (PMP) in pupariation arenas

Whereas direct observation of pupariating animals under white light is informative, barometric measurement of internal pressure changes in pupariating *Sarcophaga bullata* animals has demonstrated complex pulsations that have been correlated with different muscle contraction programs[58]. In order to perform long-term live imaging and quantitative image analyses of the muscle contraction programs that characterize pupariating behavior, we constructed a series of raspberry-pi-based behavioral arenas (Extended Data Fig. 3A, see Methods) and monitored muscle contractions of animals using a GCaMP Calcium reporter [*13XLexAop2-IVS-GCaMP6f-p10*, Ref.[59]] expressed under the control of custom-engineered muscle-specific *LexA* driver, *mhc-LHV*$_2$ [60-63] (*mhc>>GCaMP*, see Methods). *mhc>>GCaMP* animals present bright muscle-contraction-dependent green fluorescence visible under blue light in dissecting scopes (Extended Data Fig. 3B; Supplementary Video 1). Monitoring of *mhc>>GCaMP* animals in pupariation arenas allowed precise quantitative assessment of *Drosophila* pupariation behavior (Fig. 3A, B; Supplementary Video 2). The first discernable feature of pupariation is the reduction in larval locomotion behavior that precedes the onset of the pupariation motor program (PMP) by ~53.9 (23.2-82.6) min [median (25-75%)] (Fig. 3A, B, Extended Data Fig. 3C). Monitoring of *dilp8* mutants carrying the *mhc>>GCaMP* cassettes revealed no statistically significant difference in pre-PMP locomotor patterns (Extended Data Fig. 3C). Similar results were obtained for *Lgr3* mutants (Extended Data Fig. 3D). These results indicate that the pupariation problems that arise in animals lacking the Dilp8-Lgr3 pathway arise posteriorly to the triggering of the pre-PMP and likely the PMP itself.

The PMP comprises 4 distinguishable behavioral subunits (*i.e.*, stereotyped motor programs): pre-GSB, GSB, post-GSB1, and post-GSB2, (Fig. 3C), which are labeled as a function of the most discernible pupariation subprogram: glue spreading behavior (GSB), a highly stereotyped short behavior where the animal spreads ventrally the secretory glue that is expelled from the salivary gland to promote adhesion of the puparium to the substrate. This and the other behavioral subunits of PMP are further detailed in order of execution below, as well as how the absence of *dilp8* or *Lgr3* affects these subprograms.

The first stage of the PMP ("pre-GSB", Fig. 3C) is an 6.1(5.8-9.4) min-long [median(25%-75%)] motor program characterized by a series of increasingly-strong whole-body contractions, which have a characteristic number, duration, amplitude, and period (Fig. 3D-H, Extended Data Fig. 3E-K). Each contraction starts with a quasi-synchronous body muscle contraction that vigorously reduces body AR, causing the transient extrusion of the anteriormost segments, which appear negative for mhc>>GCaMP fluorescence at this stage, suggesting that the anterior segments are "squeezed" out by the increase in posterior pressure (Fig. 3I, Supplementary Video 3) After 2-4 s, large ventral intersegmental (longitudinal) muscles[64, 65] are activated and gradually retract the anteriormost segments into the body, a process that helps extrude the anterior spiracles (Fig. 3I, Supplementary Video 2). Furthermore, we noticed that the median duration of the pre-GSB contractions in WT animals increases ~10 s from the beginning to the end of the program (Extended Data Fig. 3I). Typically before the last major contraction, full and irreversible anterior retraction of the pre-spiracular segments is achieved, and the anterior segments are no longer extruded until the animal switches to the next behavioral subunit: that of glue expulsion and GSB, described in detail below.

dilp8 and Lgr3 mutants have defective pre-GSB

While all control animals surveyed performed pre-GSB, we failed to detect characteristic pre-GSB contractions in 4/21 (19.0%) *dilp8* mutants (Fig. 3E, J, K). Similar results were observed for *Lgr3* mutants (Extended Data Fig. 3E, M, N). The existence of a fraction of mutant animals that sclerotize their cuticle without any characteristic strong body remodeling contraction (Fig. 3K, Extended Data Fig. 3N), explains at least in part the very high puparium AR of some animals. The rest of the *dilp8* and *Lgr3* mutants showed pre-GSB-like

mhc>>GCaMP fluctuations that were indistinguishable in number from the pre-GSB contractions of their respective WT controls yet were significantly weaker, shorter, and more dispersed (Fig. 3E-H, Extended Data Fig. 3E-H,O-Q). Despite also increasing with time, the duration of contractions in mutant animals rarely achieved the values of control animals (Fig. 3K, Extended Data Fig. 3O). Clearly, the pre-GSB program is abnormal in *dilp8* and *Lgr3* mutants. As the *dilp8* and *Lgr3* alleles assayed are genetic nulls, and a fraction of these nulls fails to perform pre-GSB, while the other fraction fails during it, these results are consistent with our hypothesis that the Dilp8-Lgr3 pathway regulates a thresholded morphogenetic mechanism slightly before or during pre-GSB. This suggests that the function of the Dilp8-Lgr3 pathway is to control the timing of when this threshold is reached during the PMP.

Fig. 3.

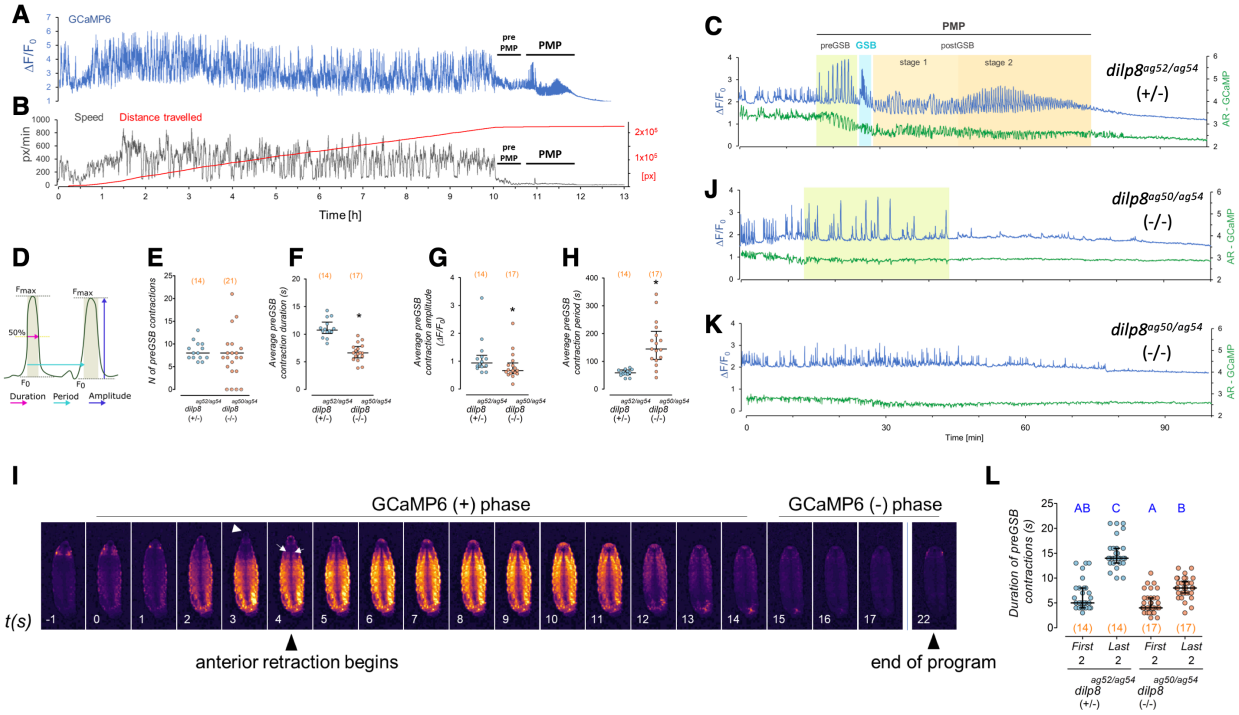

Fig. 3: Dilp8 is critical for progression of the pupariation motor program

A. Muscle calcium (mhc>>GCaMP) fluctuations (whole-body, blue), **B.** speed (black), and distance travelled by (red) a single larva. Pupariation motor program (PMP). **C,J,K.** mhc>>GCaMP (blue) and aspect ratio (AR-GCaMP, green) fluctuations in WT and **J,K.** *dilp8* mutants. **C.** PMP in (**A**) depicting stages. **D.** Parameters for pre-GSB contraction description. **E-H,L.** Dot plots showing **E.** number and average **F.** duration, **G.** amplitude, **H.** period (dot: average per larva), and **L.** duration of the first and last two pre-GSB

contractions in *dilp8* mutants and controls. **I.** Time-lapse of GCaMP oscillations during a WT pre-GSB contraction. Anteriormost segments are initially extruded (arrowhead) by the strong whole-body contraction and subsequently internalized by the activation of ventral longitudinal muscles (arrows). **J,K.** *dilp8* mutants either show pre-GSB-like contractions (**J),** or not (**K**). **L.** Statistics: Horizontal bar, **E, F-H,L.** median. Error bars: 25-75%. **E,G,H.** Mann-Whitney Rank sum test. **F.** Student's t-test. **L.** Dunn's test. **L.** Same blue letters, $P>0.05$. *$P<0.05$. $P = 0.76$ in **E** (excluding animals with no contractions). (N) Number of animals (red).

dilp8 and Lgr3 mutants do not perform GSB or post-GSB

Whereas the pre-GSB phenotypes of *dilp8* and *Lgr3* mutants are incompletely penetrant, both mutants show a 100%-penetrant failure in progressing towards GSB, the next behavioral subunit of the PMP (Fig. 4A, Supplementary Video 4). The biosynthesis and secretion of secretory glue has been studied in the context of ecdysone signaling and protein trafficking, respectively[14, 60, 66]. However, little work has been done on the behavioral context of secretory glue expulsion *per se* since the description of the behavior and the function of the glue as a cementing agent by Gottfried Fraenkel and Victor Brookes in 1953[11]. Hence, the associated motor program of GSB has not been properly described. To describe GSB in further detail, we filmed the PMP of larvae expressing the salivary gland glue protein, Sgs3, translationally fused to GFP (Sgs3::GFP) under the control of its own regulatory regions[12]. GSB has two phases, an initial tetanic contraction phase that is followed by a series of peristaltic movements that promote the expulsion and the spreading of the secretory glue onto the ventral surface of the animal (Fig. 4B, Supplementary Videos 3,5-6). The specific and sustained contraction of ventral anterior segments ("ventral tetanus" in Fig. 4B), most noticeably A2, that initiates the GSB stage slightly arches the anterior half of the larva for 17-70 *s*, depending on the larva (Fig. 4B; Supplementary Videos 5-7). This culminates with the initiation of an anterior peristaltic wave that propagates from T2 to A2 in ~3 *s*, further squeezing the anterior segments. This is followed closely (milliseconds) by the expulsion of the salivary gland contents (Fig. 4B). One or two seconds following glue expulsion, a series of coordinated peristaltic movements propagate forwards and backwards, starting from segment A2. These forth and back peristaltic movements slowly progress from A2 to posterior segments, reaching the final larval segments by the final waves (11-12 peristaltic waves in total) (Supplementary Videos 3,5,7,8). Each wave contributes to spreading the glue

towards the posterior ventral surface of the animal. During GSB, the animal typically moves forward ~half of its length, reaching its final pupariation site, where it typically waves its anterior end left and right a few times. This "head waving" marks the end of GSB. The total duration from the tetanus phase to the head waving is 71 s (62.0-86.0) [median (25-75%)] (Fig. 4C).

Fig. 4.

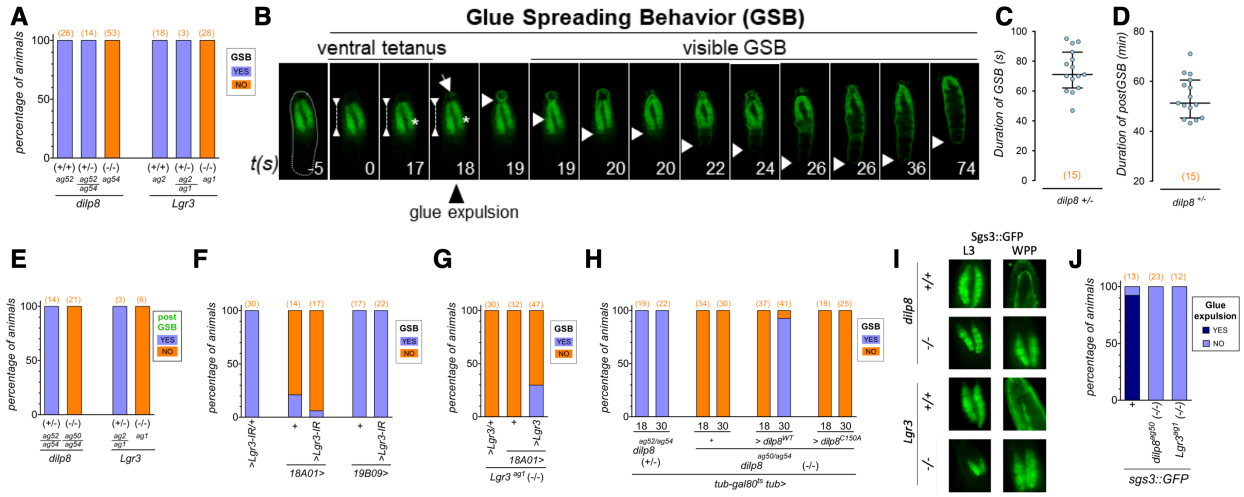

Fig. 4: Dilp8-Lgr3 pathway is required for glue expulsion and spreading behavior

A,F,G,H,J. Percentage of animals that perform GSB, **E.** post-GSB, or **J.** glue expulsion. **B.** Photo time-series of GSB and its two phases (ventral tetanus and visible GSB) in a larva expressing the salivary gland glue protein Sgs3::GFP (green) as a marker for glue (arrow, and descending white arrowhead marking progression of glue spreading towards the larval posterior, bottom). **C.** Duration of GSB and **D.** post-GSB in WT animals. Dots, one larva **E.** *dilp8* and *Lgr3* mutants fail to perform post-GSB. **F.** Knockdown of *Lgr3* in *R18A01>* neurons or *R18A01>* alone, but not in *R19B09>*, impedes GSB. **G.** Expression of *UAS-Lgr3* (*>Lgr3*) in *R18A01>* neurons partially rescues the GSB defect of *Lgr3* mutants. **H.** GSB is rescued in *dilp8* mutants by expression of Dilp8 after the MIT. **I.** *dilp8* and *Lgr3* mutants fail to expulse glue (*Sgs3::GFP,* green). **J.** Quantification of I. Statistics: **A,E,F,G,H,J.** Binomial tests with Bonferroni correction. **C,D.** Horizontal bar, median. Error bars, 25-75%. **A,F,G,H,J.** Same blue letters, (corrected *P*>0.05). (N) Number of animals (red).

To verify if GSB was a *D. melanogster*-specific behavior, we monitored pupariating *Drosophila virilis* animals in our arena. *D. virilis* flies are predicted to have shared a last common ancestor with *D. melanogaster* about 50 MYA [confidence interval (38-62 MYA)][57]. Direct observation of GSB in *D. virilis* (Supplementary Video 9), suggests that the behavior has been conserved for at least 50 MY in *Drosophila.*

The next PMP behavioral subunit, named "post-GSB" typically lasts 51.3 min (45.3-60.47) [median (25-75%)] in total and is terminated by a gradual reduction in mhc>>GCaMP-fluorescence fluctuations, which we can clearly associate with cuticle hardening, as the puparium AR no longer changes by the end of post-GSB (Fig. 3C, Fig. 4D, Supplementary Videos 8-9). *dilp8* and *Lgr3* mutants also show no visible signs of normal post-GSB (Fig. 3J, K, Fig. 4E, Extended Data Fig. 3M, N). WT post-GSB can be divided into at least two stages that are characterized by different total mhc>>GCaMP-fluorescence fluctuation patterns, post-GSB1 and post-GSB2. These stages divide post-GSB roughly in half. Both stages have complex contraction patterns, involving contraction of the whole body and the anterior longitudinal muscles. The first stage, post-GSB1, is characterized by longer, stronger, and more separated contractions than the second stage post-GSB2 (Extended Data Fig. 4A-C). While post-GSB as a whole seems to contribute to the slight reduction in AR and maintenance of the remodeled puparium shape, the functions of the post-GSB stages are not all clear. One important event that occurs during post-GSB is the formation of the operculum, from where the adult animal will exit the puparium when it is time to eclose. mhc>>GCaMP monitoring shows that operculum formation is associated with strong tetanic contraction of at least three bilateral dorsoventral muscles in segments T2, T3, and A1 and at least two large dorsal longitudinal muscles, probably of segment A2 (Extended Data Fig. 4D). Hence, operculum formation appears to be an active process requiring muscle activity, warranting further research on the regulation and evolution of this process. Clearly, this motor program is independent of *dilp8* or *Lgr3* and of progression to post-GSB, as it occurs normally in these mutants that do not perform the later. The end of post-GSB and operculum formation marks the end of the whole PMP program. At this stage, the animal has all characteristics of a WPP at T0, and the first signs of visible cuticle tanning are detectable within ~30 min.

Lgr3 is required in R18A01 neurons for GSB

To confirm that progression into GSB is also mediated by *R18A01>*-positive neurons, we scored for the presence of GSB in *R18A01>Lgr3-IR* animals. We find that *R18A01>Lgr3-IR*, but not *R19B09>Lgr3-IR*, completely abrogates GSB (Fig. 4F). However, *R18A01>* alone also partially abrogates GSB. It is therefore possible that the *R18A01>* insertion or the presence of an extra copy of the *R18A01* CRM itself interferes with GSB. As this is an *Lgr3* CRM, it could interfere with endogenous *Lgr3* levels by acting as a sponge for rate-limiting transcription factors, for instance. If this were true, GSB should be rescuable in $Lgr3^{ag1}$ animals using *R18A01>Lgr3*, the same way that puparium AR was rescuable (Fig. 1L). However, we find that while *R18A01>Lgr3* rescues AR, it only partially rescues GSB in $Lgr3^{ag1}$ animals (Fig. 4G). The fact that the GSB rescue is incomplete could suggest that *Lgr3* is an exquisitely limiting factor in the presence of *R18A01>*. Alternatively, a second factor in the *R18A01>* line could affect GSB but not AR, in an Lgr3-independent manner. Regardless, rescue of $dilp8^{ag50}$ animals by expressing *dilp8* after the MIT using the same *tub-Gal80ts, tub>dilp8* strategy that effectively rescues puparium AR (Fig. 2I), rescued GSB in 28/31 animals (Fig. 4H). We conclude that Dilp8-dependent Lgr3 activity is required in *R18A01>*-positive neurons for GSB.

The Dilp8-Lgr3 pathway is required for glue expulsion

As glue expulsion and GSB are intimately linked, and both *dilp8* and *Lgr3* mutants completely fail in performing the latter, we verified if glue expulsion was also affected by monitoring Sgs3::GFP localization in each mutant before and after pupariation (L3 wandering stage and WPP T0). Results showed that Sgs3::GFP is expulsed onto the ventral side of control WPP T0 animals, as expected, but is retained in the salivary glands of *dilp8* and *Lgr3* mutants at WPP T0 (Fig. 4I, J). Close inspection of dissected salivary glands showed that Sgs3::GFP is properly secreted into the lumen of the glands in *dilp8* and *Lgr3* WPP T0 mutants (Extended Data Fig. 4E), showing that the initial steps of glue production and secretion are unaffected in *dilp8* and *Lgr3* mutants. These results demonstrate that the Dilp8-Lgr3 pathway is required for glue expulsion and GSB.

GSB occurs independently of glue expulsion

The fact that glue expulsion fails in *dilp8* and *Lgr3* mutants could have implications for the observed pupariation phenotypes. For instance, the persistence of the enlarged salivary glands

in the body could hinder body contractions, leading to increased AR. Also, the fact that glue expulsion precedes most of the stereotypic peristaltic movements of GSB, could mean that both processes are mechanistically linked. For instance, GSB could require previous glue expulsion, *i.e.,* GSB could be a response to either external sensing of the expelled glue, or of a strong reduction in internal body pressure linked with the expulsion of the copious amounts of secretory glue. Alternatively, glue expulsion could occur independently of GSB or even be a consequence of the GSB program. To gain insight into this relationship, we hypothesized that glue expulsion was required for GSB. To test this, we performed RNAi-knockdown of the Rho GTPase *Rho1* using the salivary-gland specific driver *forkhead-GAL4* (*fkh>*). This genetic manipulation has been shown to completely block glue secretion to the lumen of the salivary gland, and hence eliminate glue expulsion[66]. We thus expected that *fkh>Rho1-IR* animals would not perform GSB. To control for the efficiency of the *fkh>Rho1-IR* genetic manipulation we monitored glue-expulsion dynamics using the Sgs3::GFP reporter. As expected, *fkh>Rho1-IR* animals completely failed in glue expulsion, retaining Sgs3::GFP in their salivary glands past the pupariation phase (Extended Data Fig. 4F). However, in contrast to our hypothesis, *fkh>Rho1-IR* animals executed GSB just as control *fkh>* animals did (Extended Data Fig. 4G) and even generated a puparia with a normal AR (Extended Data Fig. 4H). These results proved that retention of the enlarged salivary glands does not interfere with the PMP or puparium morphogenesis. We conclude that GSB occurs independently of glue expulsion. A likely scenario is that glue expulsion is triggered by the first peristaltic wave of GSB following the tetanus phase (Fig. 4B). In this case, GSB should be best defined as "glue expulsion and spreading behavior".

The Dilp8-Lgr3 pathway antagonizes cuticle sclerotization during PMP

One possibility that arises from the experiments described above is that *dilp8* mutants fail to progress in their PMP due to increased resistance of the cuticle to muscle contraction. To gain further insight into this possibility, we calculated the total PMP based on two parameters: the total duration of detectable mhc>>GCaMP fluctuations from the initiation of PMP (pre-GSB) up to the cessation/stabilization of mhc>>GCaMP fluctuations and the time it takes for the animal to cease actual AR-affecting body contractions (*i.e.,* the time from pre-GSB to complete body immobilization/sclerotization). Strikingly, whereas there was no difference in the total PMP time between *dilp8* mutants and controls, the puparium AR of

dilp8 mutants stabilized ~25 min earlier than that of controls (Fig. 5A). These results strongly suggest that the cuticle of *dilp8* mutants is hardening precociously.

Fig. 5

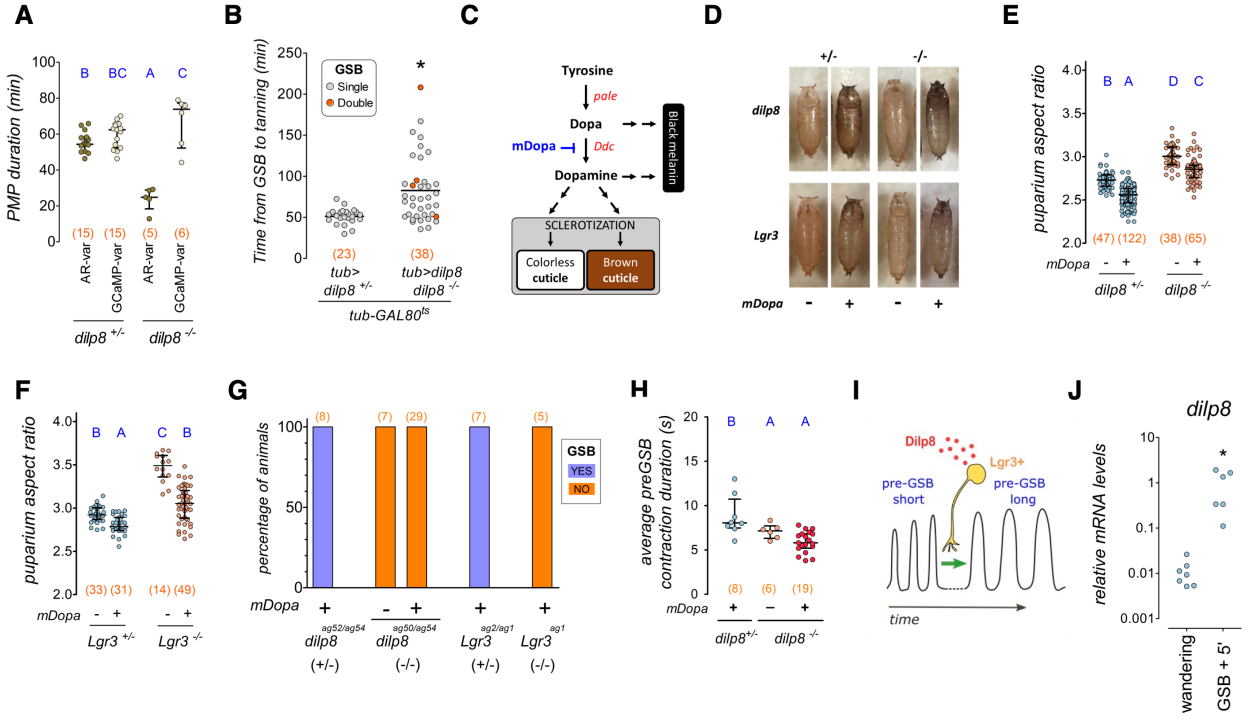

Fig. 5: Pupariation progression by coupling morphogenetic and neuromotor subprograms

A,B,E,F,H,J. Dot plots of **A.** PMP duration according to variation in puparium aspect ratio (AR-var) or GCaMP (GCaMP-var), **B.** time from GSB to tanning, **D,F.** puparium AR, **H.** average pre-GSB duration, and **J.** qRT-PCR estimations of *dilp8* mRNA levels. **A.** *dilp8*-mutant AR fluctuations are briefer than GCaMP. **B.** Post-MIT-expression of *tub>dilp8* delays tanning. **C.** Cuticle sclerotization and tanning pathway. mDopa, α-methyldopa. **D.** Photos of puparia. Effects of α-methyldopa. **E.** Quantification of **D.** for *dilp8* and **F.** *Lgr3* mutants and controls. **G,H.** α-methyldopa treatment does not **G.** rescue GSB or **H.** pre-GSB duration in mutants. **J.** Model for the Dilp8-Lgr3-dependent modulation of pre-GSB. **K.** *dilp8* mRNA levels increase 5 min after GSB. **A,B,E,F,H,J.** Dots: **A,B,E,F.** one animal, **H.** average per animal, **J.** biological repeat. **B.** Red dots, two GSBs. Statistics: **A,E,F,H.** Horizontal bar, median. Error bars, 25-75%. **A,E,F,H.** Dunn's test. **B. G.** Binomial tests with Bonferroni correction. **J.** Student's t-test.

A,B,E,F-H. Same blue letters, $P>0.05$. *$P<0.05$. (N) Number of animals (red). *dilp8(+/-) is dilp8$^{ag52/ag54}$, dilp8(-/-) is dilp8$^{ag52/ag54}$.*

If the function of the Dilp8-Lgr3 pathway is to transiently postpone cuticle sclerotization during the initial stages of the PMP, then it follows that excessive Dilp8 signaling could lead to a delay in cuticle sclerotization. To test this, we quantified the duration from GSB to detectable cuticle tanning (used here as a surrogate for sclerotization) in the *dilp8* mutants that were rescued at wandering stage with *tub>dilp8* (Fig. 4H). Results showed that *tub>dilp8*-rescued *dilp8* mutants took 31 min longer to tan than control WT animals (Fig. 5B). Tanning was delayed by >100 min in some animals (Fig. 5B). A fraction of rescued animals even executed two full PMP in tandem (Supplementary Video 10). These animals expressed crawling behavior at a time when the cuticle should have been sclerotized. Importantly, removal of animals with double GSBs or of all the animals with extreme PMP-duration values from analyses still revealed significantly-prolonged PMPs caused by *tub>dilp8* activation in wandering stage animals (28 or 12 min longer, respectively; Extended Data Fig. 5A, B). These results demonstrate that the PMP and cuticle sclerotization have been uncoupled by ectopic Dilp8 signaling and are consistent with the results indicating precocious sclerotization in *dilp8* and *Lgr3* mutants.

To independently confirm that the function of the Dilp8-Lgr3 pathway during pupariation is to transiently postpone cuticle sclerotization during the initial stages of PMP, we hypothesized that suppression of cuticle sclerotization would rescue all pupariation-related phenotypes of *dilp8* mutants. To do this, we fed α-methyldopa to *dilp8*- or *Lgr3*-mutant third-instar larvae in a concentration that attenuates cuticle sclerotization[67]. α-Methyldopa inhibits the enzyme Dopa decarboxylase (Ddc), which converts DOPA to dopamine in the epidermis, an essential step in insect cuticle sclerotization[68, 69] (Fig. 5C). α-Methyldopa treatment led to strong melanization of the cuticle, confirming that Ddc was efficiently inhibited, leading to an excess of the black-melanin precursor, DOPA (Fig. 5C, D). As predicted, α-methyldopa treatment reduced puparium AR in *dilp8* (Fig. 5E) and *Lgr3* mutants (Fig. 5F). Puparium AR was also reduced, albeit to a lesser extent, in the background controls of both mutants (Fig. 5E, F). Hence, one of the reasons why *dilp8* and *Lgr3* mutants do not achieve proper puparium AR is an excess of dopamine-mediated cuticle sclerotization, which increases the

resistance of the cuticle to underlying muscle contractions. These results also suggest that in WT animals, cuticle sclerotization must start before the PMP as it contributes as a resistance force to the body-reshaping muscle contractions of the PMP. However, α-methyldopa-fed mutants still had anterior-retraction defects and did not achieve the same AR as controls (Fig. 5D-F), suggesting that rescue by α-methyldopa treatment was not complete. These findings indicate that *dilp8* and *Lgr3* played additional roles during pupariation.

The Dilp8-Lgr3 pathway modulates the pre-GSB motor program

To gain insight into this second mechanism, we monitored mhc>>GCaMP6 in α-methyldopa-fed and vehicle-fed control animals. While α-methyldopa-fed WT animals performed all stages of PMP, including GSB, similarly to control animals (Fig. 5G, Extended Data Fig. 5C), α-methyldopa-fed *dilp8* and *Lgr3* mutants did not, remaining instead trapped in a pre-GSB-like phase, never switching to GSB (Fig. 5G, Fig S5D, E). α-Methyldopa treatment strongly increased the number of detectable pre-GSB contractions (Extended Data Fig. 5F) and mildly reduced their period (Extended Data Fig. 5G). This demonstrates that cuticle sclerotization negatively affects puparium AR by antagonizing pre-GSB number and frequency. The critical finding regarding the second mechanism, however, was that α-methyldopa treatment had little or no effect on pre-GSB contraction duration relative to untreated *dilp8* mutants (Fig. 5H, Extended Data Fig. 5E), which should increase ~10 s towards the end of the pre-GSB phase, as it does in WT animals, before anterior retraction and GSB (Fig. 3L, Fig S3I). This leads to a model where *dilp8* mutants are locked in an early, *dilp8*-independent pre-GSB-like state, which we named pre-GSB^{short}. Dilp8-Lgr3 signaling is thus required to convert the pre-GSB^{short} into the longer and stronger pre-GSB contractions, which we named pre-GSB^{long}, that typically occur at the end of the pre-GSB stage and that do not occur in *dilp8* or *Lgr3* mutants (Fig. 5I). Hence, we propose that successful anterior retraction requires both a Dilp8-dependent transient inhibition of cuticle sclerotization and the neuromodulation of the pre-GSB neuromotor contraction circuit from pre-GSB^{short} to pre-GSB^{long}. While pre-GSB^{short} can achieve some remodeling of the body it is ineffective in achieving successful anterior retraction and promoting the transit into the glue expulsion and spreading behavior phase. We further propose that successful anterior retraction is a gate to unlock the next behavioral subunit, GSB.

In order to transiently inhibit cuticle sclerotization and modulate the pre-GSB motor program, so that an effective anterior retraction is achieved, some Dilp8 protein would have to be present before the initiation of the pre-GSB program. We have shown that the peak in *dilp8* transcripts occurs around T0 (Fig. 2A), which occurs ~45-60 min after the initiation of pre-GSB (Fig. 3C). As we know that at -4 h before T0, *dilp8* mRNA levels are still flat (Extended Data Fig. 2A, C)[55], the 20HE-dependent *dilp8* upregulation must start between -4 h and T0, which is confirmed by the strong upregulation found in pre-WPP animals (Fig. 2A). However, pre-WPP can be anywhere between this ~1-h interval. To test if the *dilp8* transcripts are upregulated before T0 in a more precise manner, we obtained samples from animals exactly 5 min after they had performed GSB, a behavior that can be unequivocally scored, and compared *dilp8* mRNA levels to wandering L3 larvae by qRT-PCR. Results showed that *dilp8* mRNA levels were already upregulated by 2-3 orders of magnitude 5 min after GSB (Fig. 5J). This is consistent with the idea that enough Dilp8 protein is available for signaling events occurring 10-15 min before this time point, which corresponds to the onset of pre-GSB. This is also in line with our observations in *C. capitata*, where *cilp8* mRNA levels are already increased by a factor of ~88 in animals, which could be unequivocally-collected by eye at the ~5-min-long "body contraction" stage (Fig. 2E). Due to the obvious similarities, we assume that the *C. capitata* contraction phase corresponds to the pre-GSB stage of *D. melanogaster*. We conclude that the timing of the *ilp8* transcriptional peak is consistent with its proposed early time-window of activity during pupariation to promote PMP progression.

Lgr3 is required in 6 ventral nerve cord neurons for PMP progression

To try to further pinpoint which subpopulation of neurons is critical for proper pupariation, we took advantage of a serendipitous finding: while screening GAL4 lines for another *Lgr3*-dependent phenotype (coupling of growth and maturation), we observed elongated puparia when removing *Lgr3* using the line *R48H10-GAL4* (*R48H10>*)[52] (Fig. 6A). *R48H10>Lgr3-IR* also disrupted GSB in 100% of the animals (Fig. 6B), suggesting that *R48H10>* was active in the same cells as *R18A01>*. The relatively-sparse expression pattern of the *R48H10>* driver[52], makes it valuable for intersectional genetics. In fact, only six *R48H10>*-positive cells in the thoracic region of the CNS expressed detectable levels of Lgr3 protein, as measured by an endogenously labelled Lgr3 translational reporter [*sfGFP::Lgr3*^{ag5}, Ref.[26]] (Fig. 6C). Interestingly, six similar cells were amongst the colabelled cells when the

R18A01> line was crossed with *UAS-CD8::RFP* and *sfGFP::Lgr3^{ag5}* (Extended Data Fig. 6A).

Fig. 6.

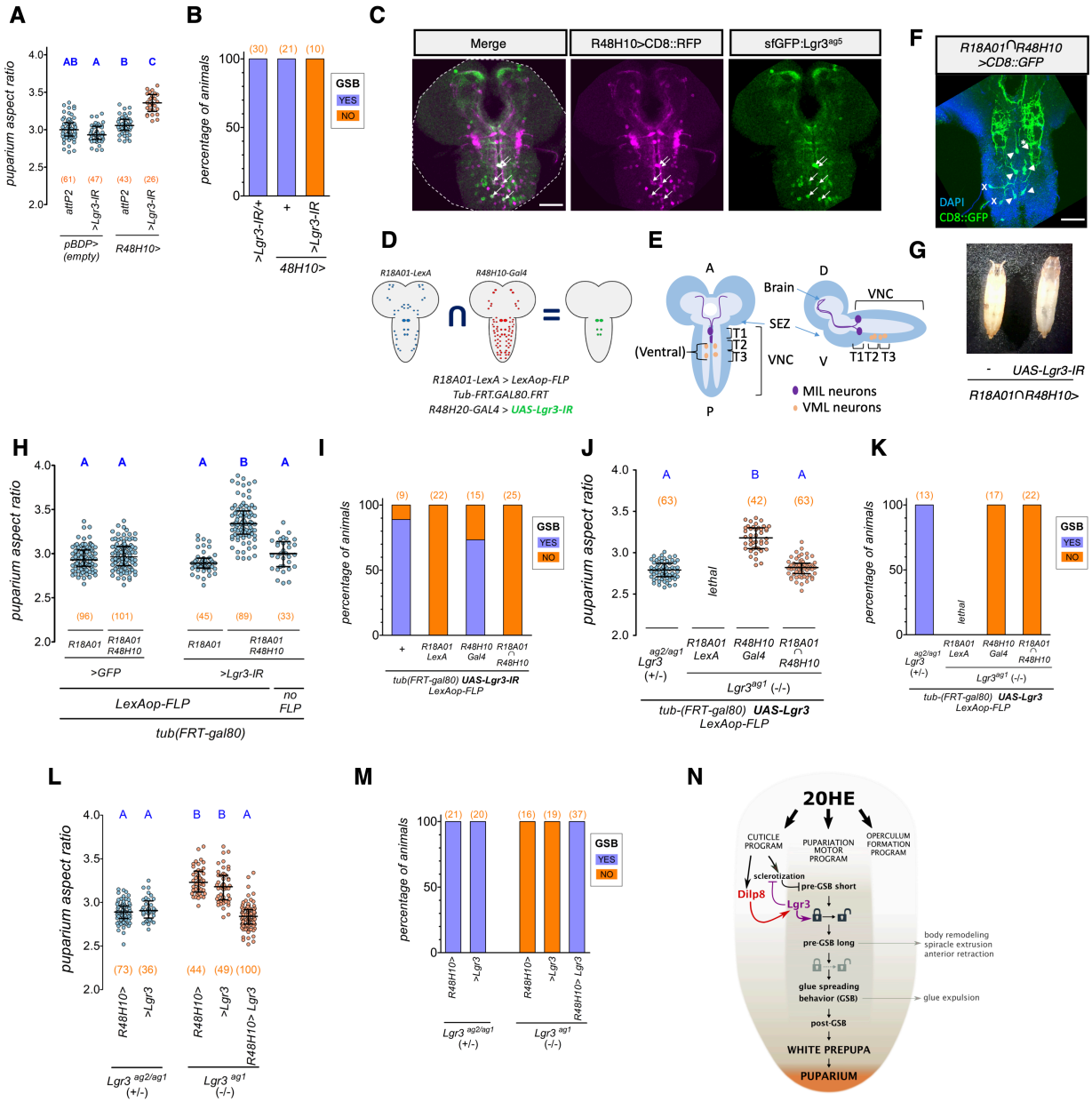

Fig. 6: Lgr3 is required in six thoracic interneurons for PMP progression

A,H,J,L. Dot plots showing puparium aspect ratio (AR). **B,I,K,N.** Percentage of animals performing GSB. **C,F.** Projections of confocal sections of white prepupa T0 CNS. **A.** *Lgr3* knockdown in *R48H10>* neurons increases puparium AR and **B.** impedes GSB. *>Lgr3-IR/+* data, same as Fig. 4C. **C.** Six thoracic (6VNC) interneurons (white arrows)

coexpress *R48H10>CD8::RFP* (magenta) and *sfGFP::Lgr3*^{ag5} (anti-GFP, green). **D.** *R18A01∩R48H10* intersectional genetics system. **E.** Cartoon of the 6VNC *R18A01∩R48H10* neurons. SEZ, subesophageal zone. T1-3, thoracic segments. **F.** 6VNC neurons (arrows) express *R18A01∩R48H10>CD8::GFP* (green). DAPI, blue. Asterisk, non-reproducible cells. **G.** Photos of *R18A01∩R48H10>Lgr3-IR* and control puparia. **H.** Quantification of **G. H.** *R18A01∩R48H10>Lgr3-IR* increases puparium AR and **I.** abrogates GSB. *R18A01-LexA* (*R18A01>>*) alone abrogates GSB. **J.** *Lgr3* expression (*UAS-Lgr3*) in *R18A01∩R48H10* or **L.** *R48H10* neurons rescues puparium AR and **K,M.** GSB in *Lgr3* mutants. **N.** Model: Dilp8-Lgr3 pathway promotes pupariation program progression. Statistics: **A,H,J,L.** Dunn's test. Horizontal bar, median. Error bars, 25-75%. **B,I,K,M.** Binomial tests with Bonferroni correction. Same blue letters, corrected *P*>0.05. (N) Number of animals (red). Scale bars, 50 µm.

To genetically confirm that these 6 neurons were co-labelled by both *R18A01>* and *R48H10>*, we generated a genetic intersection between *R18A01* and *R48H10* using a flip-out recombinase method[70] (see Methods, Extended Data Fig. 6B-D). This intersection, hereafter described as *R18A01∩R48H10*, allowed versatile usage of different UAS transgenes. As predicted from the patterns described above, *R18A01∩R48H10>CD8:GFP* consistently labelled the expected 6 VNC neurons (Fig. 6D-F). The soma of the 3 paired VNC neurons are located towards the midline of the boundaries of the T1p/T2a, and in the T2p, and T3p segments, respectively. The most anterior pair of labelled neurons has been previously described as the Midline Internal Lgr3-positive (MIL) neurons[26]. The two other pairs have not, to the best of our knowledge, been described in detail, but are always positioned ventrally, so we called them Ventral Midline Lgr3-positive (VML) neurons.

To confirm that these 6 VNC neurons require Lgr3 to promote PMP progression we used the *R18A01∩R48H10>* intersectional driver to drive *Lgr3* RNAi, and scored for puparium AR and the presence of GSB. Results revealed that *R18A01∩R48H10>Lgr3-IR* animals had increased puparium AR when compared to controls (Fig. 6G, H), and did not perform GSB (Fig. 6I), consistent with the requirement of the 6 VNC neurons for Dilp8 signaling. While all controls behaved as expected for puparium AR, the *R18A01>>* driver alone interfered with GSB (Fig. 5I). This interference was even stronger than the one found using the GAL4

version of this driver, *R18A01>,* which is inserted in a different genome location (*attp2*), excluding insertional artefacts (Fig. 4F). This confirmed our suspicion that the extra copy of the *R18A01* CRM per se interferes with normal pupariation. We again attempted to rescue the AR and GSB of $Lgr3^{ag1}$ mutants by expressing *UAS-Lgr3* under the control of *R18A01∩R48H10>*. Results showed that *R18A01∩R48H10>Lgr3* rescued puparium AR, but not GSB (Fig. 6J, K). Hence, *R18A01>>* is epistatic to *Lgr3* in GSB. To exclude the unlikely possibility that GSB is independent of the status of *Lgr3* in the 6VNC neurons, we attempted to rescue puparium AR and GSB in $Lgr3^{ag1}$ mutants using *R48H10>Lgr3* alone. The results of this rescue experiment clearly show that *R48H10>Lgr3* fully rescues puparium AR and GSB in $Lgr3^{ag1}$ mutants (Fig. 6L, M). Hence, we conclude that the *R18A01* CRM interferes with GSB specifically and epistatically to *Lgr3* function. Furthermore, we conclude that the six *R18A01∩R48H10>*-positive VNC neurons or a subset of them are the critical cells requiring Lgr3 to transduce the cuticle epidermis-derived Dilp8 signal at pupariation to promote PMP progression from pre-GSB into GSB.

Discussion

Here, we have found that the relaxin-like Dilp8-Lgr3 pathway, which has been previously shown to coordinate growth and maturation timing in earlier stages of third instar larvae[23-28, 34, 46], acts in a spatially- and temporally-independent manner during pupariation to promote pupariation motor program (PMP) progression. Epidermis-to-interneuron Dilp8-Lgr3 signaling couples peripheral tissue morphogenesis with centrally-controlled motor programs to promote progression from pre-"glue (expulsion) and spreading behavior" (pre-GSB) to "glue (expulsion) and spreading behavior" (GSB), which are the first and second behavioral subunits of the PMP. This is achieved by at least two parallel activities: by the transient inhibition of cuticle sclerotization, which promotes cuticle malleability, decreasing the resistance of the cuticle to the underlying muscle contractions, and by the neuromodulation of the Dilp8-independent pre-GSB^{short} program to a Dilp8-dependent anterior-retraction-promoting pre-GSB^{long} program. We hypothesize that both of these activities are necessary for the animal to transit from pre-GSB to the GSB phase (Fig. 6N).

We provide evidence that 20HE acts directly on the carcass to induce *dilp8* transcription, placing *dilp8* downstream of 20HE signaling. Interestingly, this is conceptually the opposite

of what Dilp8 does prior to the MIT checkpoint, where it acts upstream of 20HE production, inhibiting it[23-28, 34, 46]. However, it remains possible that Dilp8 also acts upstream of 20HE during pupariation, if the function of Dilp8-Lgr3 were to be, for instance, to inhibit vestigial 20HE signaling, contributing for instance to the termination of the 20HE peak. Even though we do not have any evidence for this, it is important to consider that Dilp8-Lgr3 signaling during pupariation controls at least two biological processes: cuticle sclerotization timing and pre-GSB neuromodulation. While both processes can be controlled by the 6 Lgr3-positive VNC neurons or by subsets of them, it is also possible that Dilp8-Lgr3 controls a third uncharacterized factor that acts upstream of these processes. While the neuroanatomy of the 4 VML neurons does not appear to favor 20HE-related activities, as they do not seem to project towards prothoracic-gland innervating neurons, the MIL neurons could affect prothoracic gland biology, and hence 20HE biosynthesis, indirectly, via their ascending projections.

Several decades ago, the insect physiologist Gottfried Fraenkel and colleagues described the "pupariation factors"[7, 71]. These are factors of peptidic nature that controlled different subprograms of pupariation downstream of the steroid hormone ecdysone in the grey flesh fly, *Sarchophaga bullata*. A pyrokinin peptide has been biochemically identified as a factor capable of accelerating pupariation initiation[22], however, its requirement *in vivo* remains to be genetically demonstrated. The identification of Dilp8 as a pupariation factor with a genetically-defined temporal and spatial role in *Drosophila* might pave the way for further identification of pupariation factors. It is unclear if Dilp8 corresponds to any of the proposed pupariation factors by Fraenkel, but it is not so dissimilar from PIF (puparium immobilization factor), due to similar profiles of expression[72]. This is further substantiated by the fact that PIF was proposed to be identical to ARF (anterior retraction factor) (a neurotropic factor that "releases behavioural patterns initiating pupariation, namely retraction of the three anterior segments bearing the cephalopharyngeal apparatus"[72], and that we show that the neurotropic peptide Dilp8 is required for fruitful anterior retraction in our study. This hypothesis is compatible with the fact that the order of body contraction and anterior retraction is inversed in *S. bullata* respective to *Drosophila*, yet the pupariation factors PIF/ARF act in a species-unspecific manner. Hence, PIF/ARF might indeed release anterior retraction after body contraction in *Drosophila*, which is what Dilp8 does by promoting transition from pre-GSB^{short} to pre-GSB^{long}. Hence, Dilp8 might as well be PIF/ARF. We hope that our work will

stimulate further evo-devo studies and allow the molecular and genetic characterization of Fraenkel's pupariation factors.

Our work, together with previous work on the role of the Dilp8-Lgr3 pathway in growth and developmental timing coordination[23-28, 34, 46], suggests that this *Drosophila* relaxin pathway can be interpreted as a bona-fide heterochronic pathway, *i.e.*, a pathway that controls the timing and/or duration of developmental processes. Heterochronic pathway genes are thought to partially contribute to the timely coordination of such programs by determining the timing of cell fate decisions cell-autonomously[73, 74]. In addition, certain hormones, such as dafachronic acid, ecdysone, and thyroid hormones, also show heterochronic-like activities by orchestrating the timing of major life history transitions, non-cell-autonomously[73, 75, 77]. Not surprisingly, these activities were revealed in animals with major clear-cut transitions, such as those undergoing metamorphosis (e.g., flies and frogs). It is unclear how other animals achieve time coordination, especially when this coordination is restricted to a subset of organs in the body. Interestingly, relaxin and relaxin-like signaling have been linked to complex developmental and behavioral programs in vertebrates, such as parturition, testicle descent, bone remodeling, and horn development in sheep[73, 78-83]. Perhaps the (re)interpretation of these programs within a heterochronic perspective could provide new insight into the evolution of relaxin-like signaling pathways and their roles in development and disease.

We found that the peripheral peptide hormone, Dilp8, modulates a central neuromotor circuit to switch a motor pattern during the execution of an innate behavior. Different types of extrinsic neuromodulators have been shown to act directly on the central nervous system. Examples are the circulating biogenic amines octopamine and serotonin that regulate posture in lobsters by acting in central circuits[84, 85], the gut-microbiota-derived tyramine that modulates an aversive olfactory response of its host, *Caenorhabditis elegans*, by acting on sensory neurons probably after being metabolized into octopamine[86], the peripheral peptides regulating feeding behavior (ghrelin, leptin, insulin, cholecystokinin, peptide YY, and pancreatic polypeptide), which directly or indirectly act on first-order feeding neurons in the hypothalamus and brainstem areas[87-90]. In insects, the ecdysis triggering hormone (ETH), which is released from inka endocrine cells and acts centrally on abdominal leucokinin

(ABLK) neurons, triggers pre-ecdysis behavior. Ecdysis is another insect innate behavior that promotes cuticle shedding. Ecdysis consists of a sequence of three behavioral subunits: pre-ecdysis, ecdysis, and post-ecdysis[91-94]. While both Dilp8 and ETH act directly on the central nervous system, the Dilp8-target neurons are interneurons, while the ABLK neurons send neurites towards the periphery, even though it is not clear if these projections are required for ETH sensing. How exactly Dilp8 transverses the blood brain barrier to reach the Lgr3-positive interneurons remains to be defined. A similar unresolved issue occurs in the earlier signaling event in the growth control paradigm, where imaginal-disc-derived peripheral Dilp8 acts on brain interneurons[23-28, 34, 46].

Drosophila Lgr3 receptor and its invertebrate orthologs are part of the ancestral group of relaxin receptors together with their vertebrate orthologs, the relaxin family receptors RXFP1 and RXFP2, which respond most specifically to the vertebrate relaxin and insulin-like peptide-3 (INSL3) ligands[46, 95]. RXFP1 and RXFP2 regulate innate behaviors and processes such as parturition and testicle-descent, respectively, amongst others. However, the vertebrate relaxin family peptide that most clearly acts as a behavioral neuromodulator is Relaxin-3, which happens to be the ancestral peptide of the vertebrate relaxin family of peptides[95]. It acts via a different receptor class, the RXFP3/4 relaxin receptor family, which is not found in invertebrates. Relaxin-3 acts as an arousal transmitter that works by altering hippocampal theta rhythms and associated learning and memory[96, 97]. While Dilp8 acts extrinsically on the CNS via an RXFP1/2-family receptor, and relaxin-3 acts intrinsically via an RXFP3/4-family receptor[96, 97], it is clear that neuromodulatory function is an ancestral function of the highly conserved relaxin family of peptides in animals.

Methods

Drosophila husbandry and stocks

Drosophila virilis (15010-1051.118 from The National Drosophila Species Stock Center) was a gift from N. Frankel. All other *Drosophila* stocks were *Drosophila melanogaster*. *UAS-dilp8* and *UAS-dilp8*^{C150A} were previously described[24]. *Lgr3*^{ag1}, *Lgr3*^{ag2}, *sfGFP::Lgr3*^{ag5}, and *UAS-Lgr3* were previously described[26]. *tub-dilp8*[27] was a gift from M. Dominguez. *Feb36-GAL4* (from C. Thummel)[98]. *w; phm-GAL4/TM6Tb,* and *y w;P0206-GAL4*[99] were gifts from C. Mirth. *ppl-GAL4*[100] and *dilp8*^{KO} [40] were gifts from P. Leopold. *nSyb-GAL4 (III)*[101] was a gift from R. Teodoro. *UAS–Rho1-IR(1)* (VDRC 12734), *UAS-Rho1-IR(2)* (*BL27727 y*^{1} *v*^{1}*; P{y[+t7.7] v[+t1.8]=TRiP.JF02809}attP2*), and *forkhead-GAL4* (*BL78060 w[*]; P{w[+mC]=fkh-GAL4.H}3*) were a gift from M. Melani. *y*^{1} *w*^{67c23}*; P(CaryP)attP40;;* was obtained from the Champalimaud Foundation Injection Facility (a gift from N. Perrimon). *UAS-dilp8-IR (v102604P dilp8-IR ({KK112161}VIE-260B))*[102] was obtained from the Vienna Drosophila Resource Center (VDRC). *vas-int; attP40 (Stock 13-20),* full genotype: *y w M(eGFP, vas-int, dmRFP)ZH-2A; P{CaryP}attP40* [103] was obtained from Fly Facility, Department of Genetics, University of Cambridge.

The following stocks were obtained from the Bloomington *Drosophila* Stock Center at Indiana University:

BL33079 y^{1} *w**; *Mi{MIC}Ilp8MI00727*
BL54591 y^{1} *M{w[+mC]=nos-Cas9.P}ZH-2A w**
BL58986 P{ry[+t7.2]=hsFLP}12, y^{1} *w**; *P{y[+t7.7] w[+mC]=UAS-Cas9.P2}attP2/TM6B, Tb*^{1}
BL49275 w^{1118}*; P{y[+t7.7] w[+mC]=GMR17G11-GAL4}attP2*
BL48786 w^{1118}*; P{y[+t7.7] w[+mC]=GMR17H01-GAL4}attP2*
BL48806 w^{1118}*; P{y[+t7.7] w[+mC]=GMR18C07-GAL4}attP2*
BL48791 w^{1118}*; P{y[+t7.7] w[+mC]=GMR18A01-GAL4}attP2*
BL48840 w^{1118}*; P{y[+t7,7] w[+mC]=GMR19B09-GAL4}attP2*
BL39171 w^{1118}*; P{y[+t7.7] w[+mC]=GMR57C10-GAL4}attP2*
BL50395 w^{1118}*; P{y[+t7.7] w[+mC]=GMR48H10-GAL4}attP2*

BL27390 y^1 w; P{w[+mC]=GAL4-Mef2.R}3*

BL44277 w^{1118}; P{y[+t7.7] w[+mC]=13XLexAop2-IVS-GCaMP6f-p10}su(Hw)attP5

BL5885 w; P{w[+m*]=Sgs3-GFP}3*

BL32219 w; P{10XUAS-IVS-mCD8::RFP}attP40*

BL55819 w^{1118}; P{y[+t7.7] w[+mC]=8XLexAop2-FLPL}attP2

BL38879 P{w[+mC]=alphaTub84B(FRT.GAL80)}1, w; Bl^1/CyO; TM2/TM6B, Tb^1*

BL32199 w^{1118}; P{10XUAS-IVS-myr::GFP}su(Hw)attP5

BL5138 y^1 w; P{w[+mC]=tubP-GAL4}LL7/TM3, Sb^1 Ser^1*

BL7016 P{w[+mC]=tubP-GAL80[ts]}Sxl[9], w[*]/FM7c

All other stocks were generated in this study as described below. Stocks are maintained at low densities at 18 °C in a 12-h light/dark cycle.

Ceratitis husbandry and sample collection

The *C. capitata* culture was kindly provided by Dr. A. Jessup and was maintained on a diet of sugar and hydrolyzed yeast protein for the adults and on a *Drosophila* food medium for the larvae. The eggs were collected and placed on the food at room temperature. After three to four days, hatching was confirmed and the bottles containing the larvae were transferred to 25 °C. Approximately 10 days after the egg lay, the larvae started to crawl out of the food at which point the bottles were placed on sawdust with the bottle caps removed. The larvae either crawled or jumped out of the bottle onto the sawdust to start the pupariation process. The larvae were collected from the sawdust and placed in a petri dish. After a period of continued crawling and jumping (wandering stage), the larvae ceased to be active and started to contract into an oblong shape (contraction stage). 1 to 1.5 h after the start of the contraction, the larvae become externally immobile (white-prepupa stage). For RNA samples, three individuals were collected in 1 ml Trizol with three replicates per time point.

Puparium aspect ratio, pupariation time measurements and pupa staging

Pictures of puparia were taken under a dissecting scope and were analyzed using ImageJ and/or Amscope software. Length was measured from the anteriormost edge of the pupa to the most anterior anal papilla (Extended Data Fig. 7A) Width was measured in the widest

part of the middle third of the pupa. Animal sex was not taken into account, because AR is equivalent in males and females, despite female puparia being proportionally longer and wider than male puparia. Pupariation time was measured essentially as previously described[26]. Animals were classified as white prepupa by direct observation through the wall of the vial. Immobile larvae were circled with a marker and regularly observed until clear signs of operculum formation were already seen (mainly, the anterior segments begin to flatten and their lateral edges thicken and become straight) but the animal was still white (Extended Data Fig. 7B).

Immunofluorescence analyses

CNS of WPP T0 animals were dissected in Schneider Medium (Biowest – cat. # L0207 or Gibco - cat. #21720-024), fixed for 30 min in 4% paraformaldehyde, rinsed with PBS with Triton (0.3%) (PBST), incubated with primary antibody overnight and with fluorescently labelled secondary antibody for 2–24 h in PBST with 1% bovine serum albumin. Samples were washed 3x for 30 min each in PBST after each antibody incubation. Nuclei were counterstained with DAPI (Sigma) and tissues were mounted in Fluoromount-G (Southern Biotech). Antibody used was: rabbit anti-GFP 1:200 (Life technologies, A11122). Images were obtained with a Zeiss LSM 710 Confocal Microscope and images were analyzed using FIJI software[104]. Typically 5–10 CNSs were mounted for observation and 1 representative image per genotype is depicted in figures. CNSs from male and female larvae were scored together.

General molecular biology

gDNA was extracted as previously described[26, 105]. Briefly, one or two flies were macerated using pellet pestles and homogenized in 100 µl DNA extraction buffer (1 M Tris-HCl at pH 8.2, 0.5 M EDTA, 5 M NaCl). Then, we added 1 µl proteinase K (final concentration of 400 µg/mL), and incubated the mixture at 37 °C for 1 h, followed by 95 °C for 5 min, to inactivate the protease.

RNA was extracted using either the Direct-zol RNA MiniPrep kit (Zymo Research), High Pure RNA Tissue Kit (Roche) or NZY Total RNA isolation kit (NZYtech), following the manufacturer's instructions. The material used for the qRT–PCR experiments described in

Fig. 2 and Fig. 5J were obtained from 1-5 staged animals, depending on the experiment, and was macerated using pellet pestles and homogenized in 800 µl of TRI Reagent or NZYol and centrifuged at 12000 g for 1 min, to lower tissue debris. After the centrifugation, half volume of absolute ethanol was added to the supernatant and mixed well. Then, the sample was loaded in a binding column of the RNA extraction kit. An extra DNAse treatment (Turbo DNA-free kit, Ambion, Life Technologies) was performed to reduce gDNA contamination. cDNA synthesis was performed using the Maxima First Strand cDNA Synthesis Kit for RT–quantitative PCR (Thermo Scientific) or NZY First-Strand cDNA Synthesis Kit, following manufacturer's instructions.

In situ hybridization probes, PCR, and qRT-PCR primers are described in their respective sections below. Briefly, their specificity was tested using Primer BLAST or Primer3. Primers and probes for *Ceratitis capitate* were obtained from InsectBase http://www.insect-genome.com/ [Whole genome assembly of Mediterranean fruit fly (Ceratitis capitata) as part of the BCM-HGSC i5k Pilot Project; Ref.[106]]. *C. capitata ilp8* (*cilp8*) corresponds to uncharacterized protein LOC101461861 [Ceratitis capitata], NCBI Reference Sequence: XP_004525593.1, Gene ID GI: 498965474. *C. capitata Rp49* (*cRp49*) corresponds to LOC101451559 60S ribosomal protein L32 [Ceratitis capitata], NCBI Reference Sequence: XP_004517954.1, Gene ID: 101451559.

20HE treatment

dilp8^{ag52} flies were left to lay eggs for 2 h on apple plates. 20 to 30 larvae were transferred to vials with normal food at 48 h after egg laying (AEL). Larvae were then collected at 96 h AEL, washed in PBS, and the carcass was dissected from the rest of the larva tissue in Schneider Medium (Gibco - cat. #21720-024). Two carcasses were incubated for each treatment in a 24-well dish. The carcasses were incubated in Schneider medium for 1 h with oxygenation by agitation (250 rpm) at room temperature (22-25°C). This timepoint corresponded to the T0 sample (before treatment). The Schneider medium was then replaced with a fresh medium containing 20-hydroxyecdysone (Cayman Chemical cat. #16145) in a final concentration of 5 µM (*49*) or equivalent volume of vehicle (absolute ethanol) for 3-6 h after which the carcass was frozen in dry ice and stored in -80 ºC conditions until processing for qRT-PCR as described above.

Treatment with mDOPA

Female flies were left to lay eggs for 6 h on egg laying plates covered with a thin layer of normal food. Thirty to 35 larvae were transferred to vials with 23 mM α-methyldopa (Hipermet, Lab Raymos) or an equivalent volume of solvent (water) 72 h AEL. Pupariation behavior of wandering larvae carrying mhc>>GCaMP was assessed in the pupariation monitoring device. The remaining larvae that pupariated in the wall of the vials were used to calculate the AR of the puparium as described above. All the experimental procedures were performed at 25 ºC.

Expression of *dilp8* after Midthird Instar Transition (MIT)

Flies were left to lay eggs for 4 h on egg laying plates covered with a thin layer of normal food at 18 ºC. Thirty to 35 larvae were transferred to vials with normal food 96 h AEL (4 d) and maintained at 18 ºC until 169 h AEL (7 d + 1 h), when they were shifted to 30 ºC. Wandering larvae were transferred to the pupariation monitoring device 4-5 h later and videos filmed at 30 ºC. As a control condition, animals with the same genotypes were bred and filmed at 18 ºC.

Preliminary experiments showed that expression of *dilp8* after 4 and 6 d of development at 18 ºC induce a ~60-h and ~40-h delay in pupariation, respectively. On the contrary, when larvae were switched to 30 ºC 7 d AEL, no delay in development was observed. Instead, *dilp8* mutants, like *Lgr3* mutants, pupariate ~4 h earlier than WT animals, as expected from their non-rescued phenotypes as regards pupariation timing control by PIL/GCL neurons[23-26]. This also suggested that the endogenous role of *dilp8* in pupariation timing control in the absence of induced imaginal disc tissue growth aberrations is played prior to the MIT.

Germline CRISPR-Cas9 generation of *dilp8* alleles

To test if the *Lgr3* puparium morphogenesis phenotype was related to the function Lgr3 plays as a receptor for Dilp8, we first quantified AR in animals carrying hypomorphic *dilp8* alleles [*dilp8*^{MI00727}, an eGFP enhancer trap[24, 105] or RNAi against *dilp8* (*dilp8-IR*[23, 24, 41]), ubiquitously-expressed under the control of a *tubulin* promoter (*tub*>), but did not observe a consistent phenotype (Extended Data Fig. 1 B-E). As it is possible that none of the hypomorphic conditions removed sufficiently enough of Dilp8 activity to affect puparium

AR, we generated *dilp8* mutants using CRISPR/Cas9-mediated directed mutagenesis[48, 49]. For this, we used a single specific guide RNA (gRNA) against *dilp8* (*dilp8*^{gRNA1}) to guide the germline Cas9 endonuclease activity (*nos-Cas9.P*)[49] to the 3' end of the *dilp8* locus, which encodes essential cysteines that are critical for Dilp8 activity[23]. We obtained 5 independent indel alleles of *dilp8* (*dilp8*^{ag50}, *dilp8*^{ag51}, *dilp8*^{ag53}, *dilp8*^{ag54}, and *dilp8*^{ag55}) all of which are predicted to severely disrupt Dilp8 activity (Extended Data Fig. 1A). One of the indels, *dilp8*^{ag50}, is a 570-bp deletion + 5-bp insertion that removes approximately half of the sequence coding for the Dilp8 carboxy-terminus (Extended Data Fig. 1A). We also kept a background control allele *dilp8*^{ag52}, where the *dilp8* sequence was intact (Extended Data Fig. 1A).

Technically, plasmid pU6-BbsI-chiRNA-dilp8_gRNA1 was generated by cloning the annealed primers #200_DILP8-GuideRNA_1_F CTTCGCACTGGTTTAGACAGCAGT and #201_DILP8-GuideRNA_1_R, AAACACTGCTGTCTAAACCAGTGC into BbsI-digested pU6-BbsI-chiRNA [a gift from Melissa Harrison & Kate O'Connor-Giles & Jill Wildonger (Addgene plasmid # 45946 ; http://n2t.net/addgene:45946 ; RRID:Addgene_45946)], as previously described[26, 48]. pU6-BbsI-chiRNA-dilp8_gRNA1 was injected into *BL54591 y*^{1} *M{w[+mC]=nos-Cas9.P}ZH-2A w** flies, after which the mutagenized 3rd chromosome was isolated by crossing to *w*^{1118}; *If/CyO; MKRS/TM6B* flies, and then to *w*^{1118};; *MKRS/TM6B* flies to select *w*^{1118};; *dilp8**/TM6B animals. Candidate indels were detected by PCR using non-*TM6B* homozygous *w*^{1118};; *dilp8** animals using primers: #107_dilp8_salto_exon2_R CAGTTGCATATGTGCCGCTGGA with primer #200 above. All recovered *dilp8* alleles were homozygous viable.

Tissue-specific CRISPR-Cas9 of *dilp8*

To genetically test if the cuticle epidermis is the primary source of Dilp8 activity that signals to Lgr3 in *R18A01* neurons to mediate proper puparium morphogenesis, we attempted to carry out tissue-specific RNAi and tissue-specific CRISPR-Cas9 experiments using a *UAS-Cas9.P2* transgene and the same *dilp8* guideRNA used for germline CRISPR-Cas9[49, 108] (generating the stock *pCFD6-dilp8*^{gRNA1}, described below) to knockdown or knockout, respectively, *dilp8* in cuticle epidermis cells. Unfortunately, these experiments were hindered by various technical limitations, such as inefficacy of *dilp8-IR* against the strong and sharp *dilp8* mRNA peak (Extended Data Fig. 1D, E), and the fact that the cuticle epidermis seems

to be particularly sensitive to toxicity effects of the Cas9.P2 endonuclease[49, 109]. Specifically, Cas9.P2 expression alone caused phenotypes that are epistatic to the puparium AR phenotype, precluding specific conclusions about the tissue-specific requirement for *dilp8* in epidermal cells of the cuticle (Extended Data Fig. 2G, H).

Generation of *pCFD6-dilp8^{gRNA1}* stock

To generate *w^{1118}; {pCFD6-dilp8^{gRNA1}}attp40;* transgenic animals, the same primary gRNA sequence used for germline CRISPR-Cas9 experiments described above was adapted and cloned into BbsI-digested *pCFD6* plasmid [a gift from Simon Bullock (Addgene plasmid # 73915 ; http://n2t.net/addgene:73915 ; RRID:Addgene_73915][108] using a primer annealing strategy with primers #681_DILP8-GuideRNA_1_F-ALT TGCAGCACTGGTTTAGACAGCAGT and #201_DILP8-GuideRNA_1_R, AAACACTGCTGTCTAAACCAGTGC. to allow *dilp8^{gRNA1}* expression under the control of *UAS* sequences. *pCFD6-dilp8^{gRNA1}* was then injected into the Drosophila stock *w M(eGFP, vas-int, dmRFP)ZH-2A; P{CaryP}attP40* for PhiC31 transgenesis (from the Champalimaud Foundation Drosophila Injection Facility). Transgenic animals were selected by eye color and balanced against *w^{1118}*; *If/CyO; MKRS/TM6B*.

Generation of the *mhc-LHV$_2$* stock

In order to generate the *mhc-LHV$_2$* stock, we amplified the *LHV$_2$* ORF (a gift from Ryohei Yagi and Konrad Basler)[63] using primers D-TOPO_LHV2_F CACCAAGCCTCCTGAAAGATG and D-TOPO_LHV2_R AATGTATCTTATCATGTCTAGAT. The ORF was then inserted into an entry vector using pENTR Directional TOPO cloning (Invitrogen) followed by Gateway cloning reaction into a *mhc* destination plasmid (mhc-Gateway, a gift from Brian McCabe). Transgenic lines were generated by standard P-element-mediated transformation procedures in a *yw* background. Insertions on the 2nd and 3rd chromosome were balanced against *w^{1118}*; *If/CyO; MKRS/TM6B*.

Generation of stock *R18A01-LexA*

To generate *y^1, w^{67c23}; P(BP_R18A01-LexA::p65Uw)attP40/CyO* (*R18A01-LexA),* we made the plasmid pBP_R18A01_LexA::p65Uw by amplifying the *R18A01* regulatory element region[50, 51] using primers #477_R18A01_Left_primer GCTTAGCCAGATTGTTGGATGCCTG and #478_R18A01_Right_primer GCGTTATGAGGTTGTGCTGCAGATC and cloning it into pBPLexA::p65Uw [a gift from Gerald Rubin (Addgene plasmid # 26231 ; http://n2t.net/addgene:26231 ; RRID:Addgene_26231)][62] using standard Gateway cloning procedures. The transgenic animals were generated by standard PhiC31 transformation[110, 111] by injecting the final plasmid into the stock *y^1 w^{67c23}; P(CaryP)attP40;;* (from the Champalimaud Foundation Drosophila Injection Facility)[103]. Transgenics were selected by eye color and balanced against *w^{1118}*; *If/CyO; MKRS/TM6B*.

Generation of stocks *13xLexAop2-GAL4v-VP48*

To generate *w^{1118}; {13xLexAop2-GAL4v-VP48}attp40;;* we made the plasmid pJFRC19-13XLexAop2-V5-GAL4v-VP48-OLLAS by substituting the XhoI-XbaI myr::GFP fragment from plasmid pJFRC19-13XLexAop2-IVS-myr::GFP [a gift from Gerald Rubin (Addgene plasmid # 26224 ; http://n2t.net/addgene:26224 ; RRID:Addgene_26224)][62] for a XhoI-XbaI V5-GAL4v-VP48-OLLAS fragment from pUC57-V5-GAL4v-VP48-OLLAS. The latter plasmid was generated by placing the following *de novo* synthesized V5-GAL4v-VP48-OLLAS (GAL4-VP48) sequence (Genscript) into EcoRV-digested pUC57. This codon-optimized and functional GAL4 transcriptional activator variant was used here due to the convenient restriction sites and its full characterization will be published elsewhere.

V5-GAL4V-VP48-OLLAS (BLUE, CAPITALIZED AND ITALICS) + flanking restriction sites (lowercase) placed into pUC57

ggtaccgaattcctcgaggccacc*ATGGGCAAGCCCATCCCGAACCCACTGCTGGGCCTGGATTC*
CACCAAGCTGCTGAGCTCCATCGAGCAGGCCTGCGACATCTGCCGCCTGAAGAAGCT
GAAGTGCTCGAAGGAGAAGCCCAAGTGCGCCAAGTGCCTGAAGAACAATTGGGAGTG
CCGCTACTCCCCCAAGACCAAGCGCTCGCCGCTGACCCGCGCCCACCTGACCGAGGT
GGAGAGCCGCCTGGAGCGCCTGGAGCAGCTGTTCCTGCTGATCTTCCCGCGCGAGG
ATCTGGACATGATCCTGAAGATGGATTCCCTGCAAGACATCAAGGCCCTGCTGACCGG
CCTGTTCGTGCAGGATAACGTGAATAAGGATGCCGTGACCGACCGCCTGGCCTCCGT

GGAGACGGACATGCCACTGACCCTGCGCCAGCACCGCATCTCGGCCACCAGCAGCA
GCGAGGAGTCGAGCAACAAGGGCCAGCGCCAGCTGACCGTGAGCGAGTTCGAGTGC
GAGTTCCTGACCCGCTCCGGCTACAGCAGCAGCGATGTGCGCGGCAAGTGCTGGGA
GCCCACCGACGCCCTGGATGACTTCGATCTGGACATGCTGCCAGCCGATGCCCTGGA
TGATTTTGATCTGGACATGCTGCCCGCCGACGCCCTGGATGATTTTGATCTGGACATGT
*TACCAGGCTCGGGATTCGCCAATGAGCTGGGACCACGCCTGATGGGCAAGTAA*gcggcc
gcggatcctctaga

The transgenic animals were generated by standard PhiC31 transformation[110, 111] by injecting the final plasmid into the stock *y*[1] *w*[67c23]*; P(CaryP)attP40;;* (from the Champalimaud Foundation Drosophila Injection Facility)[101]. Transgenics were selected by eye color and balanced against *w*[1118]; *If/CyO; MKRS/TM6B*.

Generation of the intersection stock R18A01∩R48H10>

To generate the *R18A01∩R48H10>* intersection stock, we first generated a *R180A1-LexA::p65* (*R18A01>>*) line (Extended Data Fig. 6B) as described above. In order for the intersection to work, *R18A01>>* must drive expression in the same cell types and in similar strength as the *R18A01>* version. If this is true, then knockdown of *Lgr3* by RNAi in *R18A01>>*-positive cells should increase puparium AR. To confirm this, we generated a *LexAop2-GAL4-VP48* stock and coupled it to *UAS-Lgr3-IR* transgene or to a *UAS-CD8::GFP* transgene. As expected, *R18A01>>GAL4-VP48>Lgr3-IR* strongly increased puparium AR and *R18A01>>GAL4-VP48>CD8::GFP* expression pattern was similar to the pattern obtained using *R18A01* GAL4 line (Extended Data Fig. 6C and S6D). We then coupled *R18A01>>* with *R48H10>* by adding a LexA-dependent flippase (*8x-LexAop2-FLPL*) cassette and GAL80 flip-out cassette (*alphaTub84B*(*FRT.GAL80*)), where GAL80 is flanked by FRT sites and can thus be removed by flippase recombinase activity[70]. In this way, the *R48H10>* activity is blocked in every cell except in those in which the *R18A01>>FLP* flips-out the inhibitory GAL80.

qRT-PCR

qRT–PCR experiments were performed as described previously[26]. Briefly, the experiments were performed in a Lightcycler 96 (Roche) using the FastStart Essential DNA

Green Master dye and polymerase (Roche). The final volume for each reaction was 10 µl, consisting of 5 µl of dye and polymerase (master mix), 2 µl of cDNA sample (diluted to an estimated 1-10 ng/µl equivalent of RNA) and 3 µl of the specific primer pairs.

The efficiency of the primers for the qPCR was verified by analysing a standard curve with 3 serial dilutions of gDNA from w^{1118} animals and the production of primer dimer was checked by analysing the melting curve. Only primers with more than 90% of efficiency and with no primer dimer formation were used. FastStart Essential DNA Green Master (Roche) in a LightCycler® 96 Instrument (Roche) was used for performing the PCR steps. qRT-PCR results were expressed as mRNA levels relative to *rp49* (*rp49* = 1).

The following primer pairs were used:

Drosophila melanogaster

rp49 primers

AL37_RP49-1S TGTCCTTCCAGCTTCAAGATGACCATC

AL38_RP49-1AS CTTGGGCTTGCGCCATTTGTG

dilp8 primers

AL29_CG14059 qPCR-L CGACAGAAGGTCCATCGAGT

AL30_CG14059 qPCR-R GATGCTTGTTGTGCGTTTTG

pale primers

TH_forward TTCGGAGGCGGCATTG

TH_reverse ACAGCCGACCAAGAACGATT

***Ceratitis capitata* primers**

Ccap_RpL32 (rp49)

41_Ccap_RpL32_F TAACAGAGTACGTCGTCGTTTCA

42_Ccap_RpL32_R GAATTTCTTGAAGCCAGTTGGT

Ccap_ilp8 (cilp8)

47_Ccap ilp8_p1_F TGCAAGATGAGGGTAGAGAGAAG

48_Ccap ilp8_p1_R CTTGACCCACTTTCAGATAACCA

In situ hybridization

The wandering larvae and white prepupae were cut open along the ventral midline and spread on a Sylgard petri dish in PBS. After clearing the epidermis of other tissues, it was fixed for one hour in 4% formaldehyde in PBS. The tissue was washed in PBT (PBS, 0.1% Tween-20), cut into smaller longitudinal pieces, dehydrated in 100% methanol and stored at -20 °C until use. A 413-bp fragment from *cilp8* was amplified by PCR using primers #654 cilp8_probe_fwd TGAGAACACTATTCCTTACATTCTTC and #655 cilp8_probe_rev GAAATCCTCTTCACATTTGTTGT using as template the cDNA obtained by oligodT-reverse transcriptase reaction of mRNA isolated from pupariating *C. capitata* animals. The fragment was cloned into the pGEM plasmid in a 3' to 5' direction to generate plasmid #444 pGEM-Cilp8_probe, which was used for riboprobe transcription. *In situ* hybridization was carried out as previously described[112, 113], with the following modifications: the epidermis were incubated for 3 min in 4 µg/mL proteinase K at 37°C, the hybridization buffer included heparin instead of glycogen and the hybridization step was carried out at 60 °C. Tissues were mounted in 70% glycerol in PBS and observed under the Leica DM LB2 upright microscope.

Pupariation monitoring device

The pupariation monitoring device consists of a camera connected to a Raspberry Pi microcomputer and a 3D-printed pupariation arena illuminated with LEDs.

Pupariation arenas were designed using Freecad and exported as .srt files for 3D printing. They consisted of 3 chambers of 32.0 x 12.0 x 2.0 mm, 6 chambers of 10.0 x 12.0 x 2.0 mm in a 3x2 array, or 15 chambers of 5.0 x 5.0 x 1.5 mm in a 5x3 array. All chambers were connected between them and to the outside by small grooves that were pre-designed or made with a scalpel after printing. The 6-chamber arena also had small chambers connected to each main chamber designed to contain a piece of agar to avoid larval desiccation when videos were recorded in incubators without humidity control. Larvae were filmed individually or in groups of up to six animals, depending on the size of the arena.

3D-printed arenas were placed between two pieces of glass held with metal clips or double sided adhesive tape and placed in vertical position in front of the camera of a Raspberry Pi at an adaptable focal distance. For larval monitoring under white light, two

pieces of 12-V white LED strips, each with 3 LEDs, or 6 flat 5-mm through hole LEDs (5 V, 1400 mcd, 100º) were positioned in front of the arena, above and below the camera. For *mhc>>GCaMP* transgenic larvae monitoring, two pieces of 12-V blue LED strips, each with 3 LEDs or 6 flat 5-mm through hole LEDs (5 V, 600 mcd, 100º) were used. A green filter was placed ahead of the lens of the camera to block blue light (Rosco Permacolor Dichroic Filter, #5156 Fern Green). The components of the pupariation monitoring device were assembled together using LEGO blocks or laser cut acrylic stands.

Videos were recorded at 800 x 600 or 1330 x 1000 pixel resolution when illuminated with white and blue light respectively. Up to 24-h long videos split in 5-min files were recorded using raspivid command line tool or a custom modification of the FlyPi Graphical User Interface at 10 fps[114] available in GitHub (https://github.com/AndresGarelli/FlyPi-Pupariation)

The typical settings used were:

raspivid -rot 180 -p 1050,100,800,600 -w 800 -h 600 -t 43200000 -fps 10 -b 1000000 -ex snow -sg 30000 -o nameOfFile_%04d.h264 for white light illumination and

raspivid -rot 180 -p 0,100,600,450 -w 1333 -h 1000 -t 86400000 -fps 10 -b 1000000 -ex snow -sg 300000 -sn 1 -awb off -awbg 1.3,0.1 -o nameOfFile_%04d.h264 for blue light illumination.

A detailed explanation of each parameter can be found in https://www.raspberrypi.org/documentation/raspbian/applications/camera.md

The original 5-min .h264 video files were concatenated, compressed, and saved in the .mp4 container format using ffmpeg software.

Larva tracking with ImageJ

For tracking larval behaviour, larvae were individually placed in the 3x2 arena and their movement recorded until pupariation. Videos were processed as indicated above and one frame per second was extracted and saved as a .bmp image. Position within the chamber, aspect ratio, and brightness were measured for each individual larva using a custom written ImageJ macro (Available in https://github.com/AndresGarelli/ImageJ-Larva-Tracking-Tool and as Supplementary Data 1). The data obtained was exported as a .txt file which was

further processed in Excel to calculate the actual position, speed, total distance traveled, and distance to the final position. Each parameter was calculated as follows:

- **Position:** was obtained using the centroid measurement for the larvae in each area using ImageJ.
- **Distance:** is the size in pixels of the straight line connecting two consecutive positions.
- **Total distance traveled:** is the cumulative distance the larva has traveled expressed in pixels.
- **Speed:** is calculated as the distance travelled in the previous 60 seconds.
- **Distance to final position:** the size in pixels of the straight line connecting current position with the position were the larva pupariates.

For the analysis of GCaMP fluctuations, the following parameters were calculated:

- **Duration of pre-GSB contractions:** time in seconds during which the fluorescence intensity of GCaMP is above 50% of the difference between the baseline (F_0) and maximum (F_{max}) values of each peak, where F_0 is the minimum value of the preceding 10 seconds.
- **Duration of post-GSB contractions:** time in seconds during which the fluorescence intensity of GCaMP is above a moving threshold value. A central moving minimum (CMM) was calculated as the minimum fluorescence value of a 40 seconds window centered on each point and the threshold was typically set 5% above CMM, though in some occasions that percentage was adjusted to improve peak discrimination.
- **Amplitude:** is ($\Delta F/F_0$) where ΔF is (F_{max}-F_0) and F_{max} and F_0 are the maximum and minimum fluorescence value of a peak.
- **Period:** is the time between the start of two consecutive peaks of GCaMP.

Statistical analyses

For all tests, alpha was set at 0.05 a priori. For quantitative data, comparison between multiple conditions were done using ANOVA when samples had normal distribution (Shapiro-Wilk test and equal variance). If these conditions were not met, Kruskal-Wallis One Way Analysis of Variance on Ranks was performed. If the result of these tests was

statistically significant, then Dunn's or Student-Neuwan-Keuls post-hoc tests were applied for the assessment of statistical significance of pairwise comparisons.

Comparison between two conditions were done using one-tailed unpaired (unless noted otherwise) Student's t-test, when samples had normal distribution and equal variance. Alternatively, a Mann-Whitney Rank Sum Test or Wilcoxon signed rank test (for paired samples) was performed. Statistically-significantly different comparisons were denoted with an asterisk.

For frequency (binary) data, multiple-pairwise binomial tests were performed and a Bonferonni correction was applied (alpha/number of pairwise comparisons) to assess statistical significance. Results from multiple comparisons were presented, except were explicitly denoted otherwise, with a letter scheme where conditions or genotypes sharing the same letter were not statistically significantly different.

Statistical analyses were performed either using SigmaPlot package or at https://www.socscistatistics.com/ (for binomial tests).

References:

1. Carew TJ. Behavioral neurobiology: the cellular organization of natural behavior. 2000.
2. Kim SM, Su CY, Wang JW. Neuromodulation of Innate Behaviors in Drosophila. Annu Rev Neurosci. 2017 Jul 25;40:327-348.
3. Cooke SJ, Crossin GT, Hinch SG. Pacific Salmon Migration: Completing the Cycle. In: Farrell A.P., (ed.), Encyclopedia of Fish Physiology: From Genome to Environment. San Diego: Academic Press. 2011 Jun 1; 3:1945–52.
4. Becker I, Woodley SJ, Stringer MD. The adult human pubic symphysis: a systematic review. J Anat. 2010 Nov;217(5):475-87.
5. Turner SE, Fedigan LM, Nakamichi M, Matthews HD, McKenna K, Nobuhara H, Nobuhara T, Shimizu K. Birth in free-ranging Macaca fuscata. Int J Primatol. 2010 Feb 1; 31(1);15–37.
6. Vannuccini S, Bocchi C, Severi FM, Challis JR, Petraglia F. Endocrinology of human parturition. Ann Endocrinol (Paris). 2016 Jun;77(2):105-13.
7. Denlinger DL, Zdarek J. Metamorphosis behavior of flies. Annu Rev Entomol. 1994;39:243-66.
8. Grimaldi D. & Engel M. S. Evolution of the Insects (Cambridge University Press, 2005).
9. Rolff J, Johnston PR, Reynolds S. Complete metamorphosis of insects. Philos Trans R Soc Lond B Biol Sci. 2019 Oct 14;374(1783):20190063.
10. Fraenkel G, Bhaskaran G. Pupariation and Pupation in Cyclorrhaphous Flies (Diptera): Terminology and Interpretation. Ann Entomol Soc Am. 1973 Mar 15;66(2):418–22.
11. Fraenkel G, Brookes VJ. The process by which the puparia of many species of flies become fixed to a substrate. Bio Bull. 1953 Dec;105(3):442-9.
12. Biyasheva A, Do TV, Lu Y, Vaskova M, Andres AJ. Glue secretion in the Drosophila salivary gland: a model for steroid-regulated exocytosis. Dev Biol. 2001 Mar 1;231(1):234-51.

13. Beňová-Liszeková D, Beňo M, Farkaš R. Fine infrastructure of released and solidified Drosophila larval salivary secretory glue using SEM. Bioinspir Biomim. 2019 Jul 11;14(5):055002.

14. Borne F, Kovalev A, Gorb S, Courtier-Orgogozo V. The glue produced by Drosophila melanogaster for pupa adhesion is universal. J Exp Biol. 2020 Apr 23;223(Pt 8):jeb220608.

15. Zdarek J, Fraenkel G. The mechanism of puparium formation in flies. J Exp Zool. 1972 Mar 1; 179(3):315-23.

16. Berreur P, Fraenkel G. Puparium formation in flies: contraction to puparium induced by ecdysone. Science. 1969 Jun 6;164(3884):1182-3.

17. Lam G, Thummel CS. Inducible expression of double-stranded RNA directs specific genetic interference in Drosophila. Curr Biol. 2000 Aug 24;10(16):957-63.

18. Warren JT, Yerushalmi Y, Shimell MJ, O'Connor MB, Restifo LL, Gilbert LI. Discrete pulses of molting hormone, 20-hydroxyecdysone, during late larval development of Drosophila melanogaster: correlations with changes in gene activity. Dev Dyn. 2006 Feb;235(2):315-26.

19. Zdarek J, Fraenkel G. Correlated effects of ecdysone and neurosecretion in puparium formation (pupariation) of flies. Proc Natl Acad Sci U S A. 1969 Oct;64(2):565-72.

20. Zdárek J, Denlinger DL. Neural regulation of pupariation in tsetse larvae. J Exp Biol. 1992 Dec;173:11-24.

21. Zdarek J, Nachman RJ, Hayes TK. Insect neuropeptides of the pyrokinin/PBAN family accelerate pupariation in the fleshfly (Sarcophaga bullata) larvae. Ann N Y Acad Sci. 1997 Apr 24;814:67-72.

22. Verleyen P, Clynen E, Huybrechts J, Van Lommel A, Vanden Bosch L, De Loof A, Zdarek J, Schoofs L. Fraenkel's pupariation factor identified at last. Dev Biol. 2004 Sep 1;273(1):38-47.

23. Colombani J, Andersen DS, Léopold P. Secreted peptide Dilp8 coordinates Drosophila tissue growth with developmental timing. Science. 2012 May 4;336(6081):582-5.

24. Garelli A, Gontijo AM, Miguela V, Caparros E, Dominguez M. Imaginal discs secrete insulin-like peptide 8 to mediate plasticity of growth and maturation. Science. 2012 May 4;336(6081):579-82.

25. Colombani J, Andersen DS, Boulan L, Boone E, Romero N, Virolle V, Texada M, Léopold P. Drosophila Lgr3 Couples Organ Growth with Maturation and Ensures Developmental Stability. Curr Biol. 2015 Oct 19;25(20):2723-9.

26. Garelli A, Heredia F, Casimiro AP, Macedo A, Nunes C, Garcez M, Dias ARM, Volonte YA, Uhlmann T, Caparros E, Koyama T, Gontijo AM. Dilp8 requires the neuronal relaxin receptor Lgr3 to couple growth to developmental timing. Nat Commun. 2015 Oct 29;6:8732.

27. Vallejo DM, Juarez-Carreño S, Bolivar J, Morante J, Dominguez M. A brain circuit that synchronizes growth and maturation revealed through Dilp8 binding to Lgr3. Science. 2015 Nov 13;350(6262):aac6767.

28. Jaszczak JS, Wolpe JB, Bhandari R, Jaszczak RG, Halme A. Growth Coordination During Drosophila melanogaster Imaginal Disc Regeneration Is Mediated by Signaling Through the Relaxin Receptor Lgr3 in the Prothoracic Gland. Genetics. 2016 Oct;204(2):703-709.

29. Parker NF, Shingleton AW. The coordination of growth among Drosophila organs in response to localized growth-perturbation. Dev Biol. 2011 Sep 15;357(2):318-25.

30. Russell MA. Pattern formation in the imaginal discs of a temperature-sensitive cell-lethal mutant of Drosophila melanogaster. Dev Biol. 1974 Sep;40(1):24-39.

31. Simpson P, Schneiderman HA. Isolation of temperature sensitive mutations blocking clone development in Drosophila melanogaster, and the effects of a temperature sensitive cell lethal mutation on pattern formation in imaginal discs. Wilehm Roux Arch Dev Biol. 1975 Sep;178(3):247-275.

32. Simpson P, Berreur P, Berreur-Bonnenfant J. The initiation of pupariation in Drosophila: dependence on growth of the imaginal discs. J Embryol Exp Morphol. 1980 Jun;57:155-65.

33. Halme A, Cheng M, Hariharan IK. Retinoids regulate a developmental checkpoint for tissue regeneration in Drosophila. Curr Biol. 2010 Mar 9;20(5):458-63.

34. Hackney JF, Zolali-Meybodi O, Cherbas P. Tissue damage disrupts developmental progression and ecdysteroid biosynthesis in Drosophila. PLoS One. 2012;7(11):e49105.

35. Klebes A, Sustar A, Kechris K, Li H, Schubiger G, Kornberg TB. Regulation of cellular plasticity in Drosophila imaginal disc cells by the Polycomb group, trithorax group and lama genes. Development. 2005 Aug;132(16):3753-65.

36. Demay Y, Perochon J, Szuplewski S, Mignotte B, Gaumer S. The PERK pathway independently triggers apoptosis and a Rac1/Slpr/JNK/Dilp8 signaling favoring tissue homeostasis in a chronic ER stress Drosophila model. Cell Death Dis. 2014 Oct 9;5:e1452.

37. Katsuyama T, Comoglio F, Seimiya M, Cabuy E, Paro R. During Drosophila disc regeneration, JAK/STAT coordinates cell proliferation with Dilp8-mediated developmental delay. Proc Natl Acad Sci U S A. 2015 May 5;112(18):E2327-36.

38. Külshammer E, Mundorf J, Kilinc M, Frommolt P, Wagle P, Uhlirova M. Interplay among Drosophila transcription factors Ets21c, Fos and Ftz-F1 drives JNK-mediated tumor malignancy. Dis Model Mech. 2015 Oct 1;8(10):1279-93.

39. Skinner A, Khan SJ, Smith-Bolton RK. Trithorax regulates systemic signaling during Drosophila imaginal disc regeneration. Development. 2015 Oct 15;142(20):3500-11.

40. Boone E, Colombani J, Andersen DS, Léopold P. The Hippo signalling pathway coordinates organ growth and limits developmental variability by controlling dilp8 expression. Nat Commun. 2016 Nov 22;7:13505.

41. Boulan L, Andersen D, Colombani J, Boone E, Léopold P. Inter-Organ Growth Coordination Is Mediated by the Xrp1-Dilp8 Axis in Drosophila. Dev Cell. 2019 Jun 3;49(5):811-818.e4.

42. Sanchez JA, Mesquita D, Ingaramo MC, Ariel F, Milán M, Dekanty A. Eiger/TNFα-mediated Dilp8 and ROS production coordinate intra-organ growth in Drosophila. PLoS Genet. 2019 Aug 19;15(8):e1008133.

43. Hariharan IK. How growth abnormalities delay "puberty" in Drosophila. Sci Signal. 2012 Jun 19;5(229):pe27.

44. Hackney JF, Cherbas P. Injury response checkpoint and developmental timing in insects. Fly (Austin). 2014;8(4):226-31.

45. Juarez-Carreño S, Morante J, Dominguez M. Systemic signalling and local effectors in developmental stability, body symmetry, and size. Cell Stress. 2018 Nov 13;2(12):340-361.

46. Gontijo AM, Garelli A. The biology and evolution of the Dilp8-Lgr3 pathway: A relaxin-like pathway coupling tissue growth and developmental timing control. Mech Dev. 2018 Dec;154:44-50.

47. Garelli A, Heredia F, Casimiro AP, Macedo A, Nunes C, Koyama T, Gontijo AM. Dilp8 requires the neuronal relaxin receptor Lgr3 to couple growth to developmental timing. bioRxiv 2015 Mar 25; 017053.

48. Gratz SJ, Cummings AM, Nguyen JN, Hamm DC, Donohue LK, Harrison MM, Wildonger J, O'Connor-Giles KM. Genome engineering of Drosophila with the CRISPR RNA-guided Cas9 nuclease. Genetics. 2013 Aug;194(4):1029-35.

49. Port F, Chen HM, Lee T, Bullock SL. Optimized CRISPR/Cas tools for efficient germline and somatic genome engineering in Drosophila. Proc Natl Acad Sci U S A. 2014 Jul 22;111(29):E2967-76.

50. Pfeiffer BD, Jenett A, Hammonds AS, Ngo TT, Misra S, Murphy C, Scully A, Carlson JW, Wan KH, Laverty TR, Mungall C, Svirskas R, Kadonaga JT, Doe CQ, Eisen MB, Celniker SE, Rubin GM. Tools for neuroanatomy and neurogenetics in Drosophila. Proc Natl Acad Sci U S A. 2008 Jul 15;105(28):9715-20.

51. Pfeiffer BD, Truman JW, Rubin GM. Using translational enhancers to increase transgene expression in Drosophila. Proc Natl Acad Sci U S A. 2012 Apr 24;109(17):6626-31.

52. Jenett A, Rubin GM, Ngo TT, Shepherd D, Murphy C, Dionne H, Pfeiffer BD, Cavallaro A, Hall D, Jeter J, Iyer N, Fetter D, Hausenfluck JH, Peng H, Trautman ET, Svirskas RR, Myers EW, Iwinski ZR, Aso Y, DePasquale GM, Enos A, Hulamm P, Lam SC, Li HH, Laverty TR, Long F, Qu L, Murphy SD, Rokicki K, Safford T, Shaw K, Simpson JH, Sowell A, Tae S, Yu Y, Zugates CT. A GAL4-driver line resource for Drosophila neurobiology. Cell Rep. 2012 Oct 25;2(4):991-1001.

53. Li HH, Kroll JR, Lennox SM, Ogundeyi O, Jeter J, Depasquale G, Truman JW. A GAL4 driver resource for developmental and behavioral studies on the larval CNS of Drosophila. Cell Rep. 2014 Aug 7;8(3):897-908.

54. Li TR, White KP. Tissue-specific gene expression and ecdysone-regulated genomic networks in Drosophila. Dev Cell. 2003 Jul;5(1):59-72.

55. Beckstead RB, Lam G, Thummel CS. The genomic response to 20-hydroxyecdysone at the onset of Drosophila metamorphosis. Genome Biol. 2005;6(12):R99.

56. Brown JB, Boley N, Eisman R, May GE, Stoiber MH, Duff MO, Booth BW, Wen J, Park S, Suzuki AM, Wan KH, Yu C, Zhang D, Carlson JW, Cherbas L, Eads BD, Miller D, Mockaitis K, Roberts J, Davis CA, Frise E, Hammonds AS, Olson S, Shenker S, Sturgill D, Samsonova AA, Weiszmann R, Robinson G, Hernandez J, Andrews J, Bickel PJ, Carninci P, Cherbas P, Gingeras TR, Hoskins RA, Kaufman TC, Lai EC, Oliver B, Perrimon N, Graveley BR, Celniker SE. Diversity and dynamics of the Drosophila transcriptome. Nature. 2014 Aug 28;512(7515):393-9.

57. Kumar S, Stecher G, Suleski M, Hedges SB. TimeTree: A Resource for Timelines, Timetrees, and Divergence Times. Mol Biol Evol. 2017 Jul 1;34(7):1812-1819.

58. Zdarek J, Slama K, Fraenkel G. Changes in internal pressure during puparium formation in flies. J Exp Zool. 1979. 207:187-96.

59. Chen TW, Wardill TJ, Sun Y, Pulver SR, Renninger SL, Baohan A, Schreiter ER, Kerr RA, Orger MB, Jayaraman V, Looger LL, Svoboda K, Kim DS. Ultrasensitive fluorescent proteins for imaging neuronal activity. Nature. 2013 Jul 18;499(7458):295-300.

60. Szüts D, Bienz M. LexA chimeras reveal the function of Drosophila Fos as a context-dependent transcriptional activator. Proc Natl Acad Sci U S A. 2000 May 9;97(10):5351-6.

61. Lai SL, Lee T. Genetic mosaic with dual binary transcriptional systems in Drosophila. Nat Neurosci. 2006 May;9(5):703-9.

62. Pfeiffer BD, Ngo TT, Hibbard KL, Murphy C, Jenett A, Truman JW, Rubin GM. Refinement of tools for targeted gene expression in Drosophila. Genetics. 2010 Oct;186(2):735-55.

63. Yagi R, Mayer F, Basler K. Refined LexA transactivators and their use in combination with the Drosophila Gal4 system.Proc Natl Acad Sci U S A. 2010 Sep 14;107(37):16166-71.

64. Hooper JE. Homeotic gene function in the muscles of Drosophila larvae. EMBO J. 1986 Sep;5(9):2321-2329.

65. Wipfler B, Schneeberg K, Löffler A, Hünefeld F, Meier R, Beutel RG. The skeletomuscular system of the larva of Drosophila melanogaster (Drosophilidae, Diptera): a contribution to the morphology of a model organism. Arthropod Struct Dev. 2013 Jan;42(1):47-68.

66. Rousso T, Schejter ED, Shilo BZ. Orchestrated content release from Drosophila glue-protein vesicles by a contractile actomyosin network. Nat Cell Biol. 2016;18(2):181-190.

67. Wright TR. The Genetics of Dopa Decarboxylase and α-Methyl Dopa Sensitivity in Drosophila melanogaster. Amer Zool. 1977. 17:707-21.

68. Sugumaran M, Barek H. Critical Analysis of the Melanogenic Pathway in Insects and Higher Animals. Int J Mol Sci. 2016 Oct 20;17(10).

69. Andersen SO. Insect cuticular sclerotization: a review. Insect Biochem Mol Biol. 2010 Mar;40(3):166-78.

70. Gordon MD, Scott K. Motor control in a Drosophila taste circuit. Neuron. 2009 Feb 12;61(3):373-84.

71. Fraenkel G, Zdarek J, Sivasubramanian P. Hormonal factors in the CNS and hemolymph of pupariating fly larvae which accelerate puparium formation and tanning. Biol Bull. 1972 Aug;143(1):127-39.

72. Zdarek J, Rohle R, Blechi J, Fraenkel G. A hormone effecting immobilization in pupariating fly larvae. J Exp Biol 1981;93:51–63.

73. Moss EG. Heterochronic genes and the nature of developmental time. Curr Biol. 2007;17(11):R425-R434.

74. Moss EG, Romer-Seibert J. Cell-intrinsic timing in animal development. Wiley Interdiscip Rev Dev Biol. 2014 Sep-Oct;3(5):365-77.

75. Frieden E. The dual role of thyroid hormones in vertebrate development and calorigenesis. in: Gilbert L.I. Frieden E. Metamorphosis: A Problem in Developmental Biology. Plenum, New York. 1981: 545-64.

76. Thummel CS. Molecular mechanisms of developmental timing in C. elegans and Drosophila. Dev Cell. 2001 Oct;1(4):453-65.

77. Rottiers V, Antebi A. Control of Caenorhabditis elegans life history by nuclear receptor signal transduction. Exp Gerontol. 2006 Oct;41(10):904-9.

78. Zimmermann S, Steding G, Emmen JM, Brinkmann AO, Nayernia K, Holstein AF, Engel W, Adham IM. Targeted disruption of the Insl3 gene causes bilateral cryptorchidism. Mol Endocrinol. 1999 May;13(5):681-91.

79. Kumagai J, Hsu SY, Matsumi H, Roh JS, Fu P, Wade JD, Bathgate RA, Hsueh AJ. INSL3/Leydig insulin-like peptide activates the LGR8 receptor important in testis descent. J Biol Chem. 2002 Aug 30;277(35):31283-6.

80. Ferlin A, Pepe A, Gianesello L, Garolla A, Feng S, Giannini S, Zaccolo M, Facciolli A, Morello R, Agoulnik AI, Foresta C. Mutations in the insulin-like factor 3 receptor are associated with osteoporosis. J Bone Miner Res. 2008 May;23(5):683-93.

81. Kijas JW, Lenstra JA, Hayes B, Boitard S, Porto Neto LR, San Cristobal M, Servin B, McCulloch R, Whan V, Gietzen K, Paiva S, Barendse W, Ciani E, Raadsma H, McEwan J, Dalrymple B; International Sheep Genomics Consortium Members. Genome-wide analysis of the world's sheep breeds reveals high levels of historic mixture and strong recent selection. PLoS Biol. 2012 Feb;10(2):e1001258.

82. Wiedemar N, Drögemüller C. A 1.8-kb insertion in the 3'-UTR of RXFP2 is associated with polledness in sheep. Anim Genet. 2015 Aug;46(4):457-61.

83. Johnston SE, Gratten J, Berenos C, Pilkington JG, Clutton-Brock TH, Pemberton JM, Slate J. Life history trade-offs at a single locus maintain sexually selected genetic variation. Nature. 2013 Oct 3;502(7469):93-5.

84. Harris-Warrick RM, Kravitz EA. Cellular mechanisms for modulation of posture by octopamine and serotonin in the lobster. J Neurosci. 1984;4(8):1976-1993.

85. Marder E. Neuromodulation of neuronal circuits: back to the future. Neuron. 2012 Oct 4;76(1):1-11.

86. O'Donnell MP, Fox BW, Chao PH, Schroeder FC, Sengupta P. A neurotransmitter produced by gut bacteria modulates host sensory behaviour. Nature. 2020;583(7816):415-420.

87. Zhang Y, Proenca R, Maffei M, Barone M, Leopold L, Friedman JM. Positional cloning of the mouse obese gene and its human homologue [published correction appears in Nature 1995 Mar 30;374(6521):479]. Nature. 1994;372(6505):425-432.

88. Comeras LB, Herzog H, Tasan RO. Neuropeptides at the crossroad of fear and hunger: a special focus on neuropeptide Y. Ann N Y Acad Sci. 2019;1455(1):59-80.

89. Münzberg H, Singh P, Heymsfield SB, Yu S, Morrison CD. Recent advances in understanding the role of leptin in energy homeostasis. F1000Res. 2020;9:F1000 Faculty Rev-451.

90. Izquierdo AG, Crujeiras AB, Casanueva FF, Carreira MC. Leptin, Obesity, and Leptin Resistance: Where Are We 25 Years Later? Nutrients. 2019 Nov 8;11(11):2704.

91. Zitnan D, Adams ME. Neuroendocrine regulation of ecdysis. In: Insect Endocrinology, Academic Press. 2012 Jan 1;253-309.

92. Krüger E, Mena W, Lahr EC, Johnson EC, Ewer J. Genetic analysis of Eclosion hormone action during Drosophila larval ecdysis. Development. 2015;142(24):4279-4287.

93. Kim DH, Han MR, Lee G, Lee SS, Kim YJ, Adams ME. Rescheduling Behavioral Subunits of a Fixed Action Pattern by Genetic Manipulation of Peptidergic Signaling. PLoS Genet. 2015 Sep 24;11(9):e1005513.

94. Diao F, Elliott AD, Diao F, Shah S, White BH. Neuromodulatory connectivity defines the structure of a behavioral neural network. Elife. 2017;6:e29797.

95. Bathgate RAD, Kocan M, Scott DJ, Hossain MA, Good SV, Yegorov S, Bogerd J, Gooley PR. The relaxin receptor as a therapeutic target - perspectives from evolution and drug targeting. Pharmacol Ther. 2018 Jul;187:114-132.

96. Smith CM, Walker AW, Hosken IT, Chua BE, Zhang C, Haidar M, Gundlach AL. Relaxin-3/RXFP3 networks: an emerging target for the treatment of depression and other neuropsychiatric diseases? Front Pharmacol. 2014 Mar 21;5:46.

97. Olucha-Bordonau FE, Albert-Gascó H, Ros-Bernal F, Rytova V, Ong-Pålsson EKE, Ma S, Sánchez-Pérez AM, Gundlach AL. Modulation of forebrain function by nucleus incertus and relaxin-3/RXFP3 signaling. CNS Neurosci Ther. 2018 Aug;24(8):694-702.

98. Siegmund T, Korge G. Innervation of the ring gland of Drosophila melanogaster. J Comp Neurol. 2001 Mar 19;431(4):481-91.

99. Mirth C, Truman JW, Riddiford LM. The role of the prothoracic gland in determining critical weight for metamorphosis in Drosophila melanogaster. Curr Biol. 2005;15(20):1796-1807.

100. Buch S, Melcher C, Bauer M, Katzenberger J, Pankratz MJ. Opposing effects of dietary protein and sugar regulate a transcriptional target of Drosophila insulin-like peptide signaling. Cell Metab. 2008 Apr;7(4):321-32.

101. Simpson JH. Rationally subdividing the fly nervous system with versatile expression reagents. J Neurogenet. 2016 Sep - Dec;30(3-4):185-194.

102. Dietzl G, Chen D, Schnorrer F, Su KC, Barinova Y, Fellner M, Gasser B, Kinsey K, Oppel S, Scheiblauer S, Couto A, Marra V, Keleman K, Dickson BJ. A genome-wide transgenic RNAi library for conditional gene inactivation in Drosophila. Nature. 2007 Jul 12;448(7150):151-6.

103. Bischof J, Maeda RK, Hediger M, Karch F, Basler K. An optimized transgenesis system for Drosophila using germ-line-specific phiC31 integrases. Proc Natl Acad Sci U S A. 2007 Feb 27;104(9):3312-7.

104. Schindelin J, Arganda-Carreras I, Frise E, Kaynig V, Longair M, Pietzsch T, Preibisch S, Rueden C, Saalfeld S, Schmid B, Tinevez JY, White DJ, Hartenstein V, Eliceiri K, Tomancak P, Cardona A. Fiji: an open-source platform for biological-image analysis. Nat Methods. 2012 Jun 28;9(7):676-82.

105. Carvalho GB, Ja WW, Benzer S. Non-lethal PCR genotyping of single Drosophila. Biotechniques. 2009;46(4):312-314.

106. Yin C, Shen G, Guo D, et al. InsectBase: a resource for insect genomes and transcriptomes. Nucleic acids research, 2016, 44(D1): D801-D807.

107. Nagarkar-Jaiswal S, Lee PT, Campbell ME, Chen K, Anguiano-Zarate S, Gutierrez MC, Busby T, Lin WW, He Y, Schulze KL, Booth BW, Evans-Holm M, Venken KJ, Levis RW, Spradling AC, Hoskins RA, Bellen HJ. A library of MiMICs allows tagging of genes and reversible, spatial and temporal knockdown of proteins in Drosophila. Elife. 2015 Mar 31;4.

108. Port F, Bullock SL. Augmenting CRISPR applications in Drosophila with tRNA-flanked sgRNAs. Nat Methods. 2016 Oct;13(10):852-4.

109. Port F, Strein C, Stricker M, Rauscher B, Heigwer F, Zhou J, Beyersdörffer C, Frei J, Hess A, Kern K, Lange L, Langner N, Malamud R, Pavlovic B, Rädecke K, Schmitt L, Voos L, Valentini E, Boutros M. A large-scale resource for tissue-specific CRISPR mutagenesis in Drosophila. Elife. 2020 Feb 13;9. pii: e53865.

110. Groth AC, Fish M, Nusse R, Calos MP. Construction of transgenic Drosophila by using the site-specific integrase from phage phiC31. Genetics. 2004 Apr;166(4):1775-82.
111. Markstein M, Pitsouli C, Villalta C, Celniker SE, Perrimon N. Exploiting position effects and the gypsy retrovirus insulator to engineer precisely expressed transgenes. Nat Genet. 2008 Apr;40(4):476-83.
112. Panganiban G, Sebring A, Nagy L, Carroll S. The development of crustacean limbs and the evolution of arthropods. Science. 1995 Nov 24;270(5240):1363-6.
113. Tautz D, Pfeifle C. A non-radioactive in situ hybridization method for the localization of specific RNAs in Drosophila embryos reveals translational control of the segmentation gene hunchback. Chromosoma. 1989 Aug;98(2):81-5.
114. Maia Chagas A, Prieto-Godino LL, Arrenberg AB, Baden T. The €100 lab: A 3D-printable open-source platform for fluorescence microscopy, optogenetics, and accurate temperature control during behaviour of zebrafish, Drosophila, and Caenorhabditis elegans. PLoS Biol. 2017 Jul 18;15(7):e2002702.

Acknowledgments

We thank Drs. Carlos Ribeiro, Christen Mirth, Elio Sucena, Filip Port, Frank Schnorrer, Julien Colombani, Maria Dominguez, Maria Luisa Vasconcelos, Pierre Leopold, Simon Bullock, Rita Teodoro, Gerald Rubin, Melissa Harrison, Kate O'Connor-Giles, Jill Wildonger, Mariana Melani, Pablo Wappner and Christian Wegener for fly stocks and reagents. We thank Ryohei Yagi and Konrad Basler for the *LHV$_2$* plasmid and Brain McCabe for the *mhc*-Gateway destination plasmid. We thank Carlos Ribeiro, Dennis Goldschmidt and Marcos Dibo for help in designing and constructing one of the pupariation arenas and Mariana Melani and Pablo Wappner for sharing resources and unpublished data. We thank Arash Bashirullah and Carlos Ribeiro for discussions and comments on the manuscript, and Jim Truman for discussions on Fraenkel's pupariation factors. Work in the Integrative Biomedicine Laboratory was supported by the European Commission FP7 (PCIG13-GA-2013-618847), by the FCT (IF/00022/2012; Congento LISBOA-01-0145-FEDER-022170, co-financed by FCT/Lisboa2020; UID/Multi/04462/2019; PTDC/BEXBCM/1370/2014; PTDC/MED-NEU/30753/2017; PTDC/BIA-BID/31071/2017; FCT SFRH/BPD/94112/2013; SFRH/BD/94931/2013), the MIT Portugal Program (MIT-EXPL/BIO/0097/2017), and FAPESP (16/09659-3, 16/10342-4, and 17/17904-0). AG is a CONICET researcher, YV holds a CONICET postdoctoral fellowship and FPS and MJD hold a PhD fellowship from

CONICET. Work in the Garelli lab was supported by ANPCyT (Agencia Nacional para la Promoción de la Ciencia y la Tecnología, PICT 2014-2900 and PICT 2017-0254) and CONICET (PIP11220150100182CO).

Author contribution

FH, YV, JP, MF,MA, FHPS,MJD, and AG performed genetic, phenotypic, molecular, and behavioral experiments. FH, YV, APC, AM, RDM, AG, and AMG generated and characterized mutants. KT, FH, and GAC performed Ceratitis experiments. FH, YV, CB, MF, and AG performed qRT-PCRs. FV contributed to genetic and phenotypic characterization; JP, MF, MK, MJD, AG, and AMG built pupariation arenas and contributed to behavioral analyses under supervision of AG; MK and AG wrote scripts; CSM developed critical reagents. FH, TTT, AG, and AMG supervised the work. AG and AMG contributed to image and data analyses and wrote the manuscript with the help of all authors.

Author information

The authors declare no competing financial interests. Correspondence and requests for materials should be addressed to agarelli@inibibb-conicet.gob.ar (A.G.) and alisson.gontijo@nms.unl.pt (A.M.G.).

Supplementary Information:

Extended Data Fig. 1 – 7

Supplementary Videos 1-10

Supplementary Data 1 (.rar file containing Github files of our code)

Extended Data

Extended Data Figure 1.

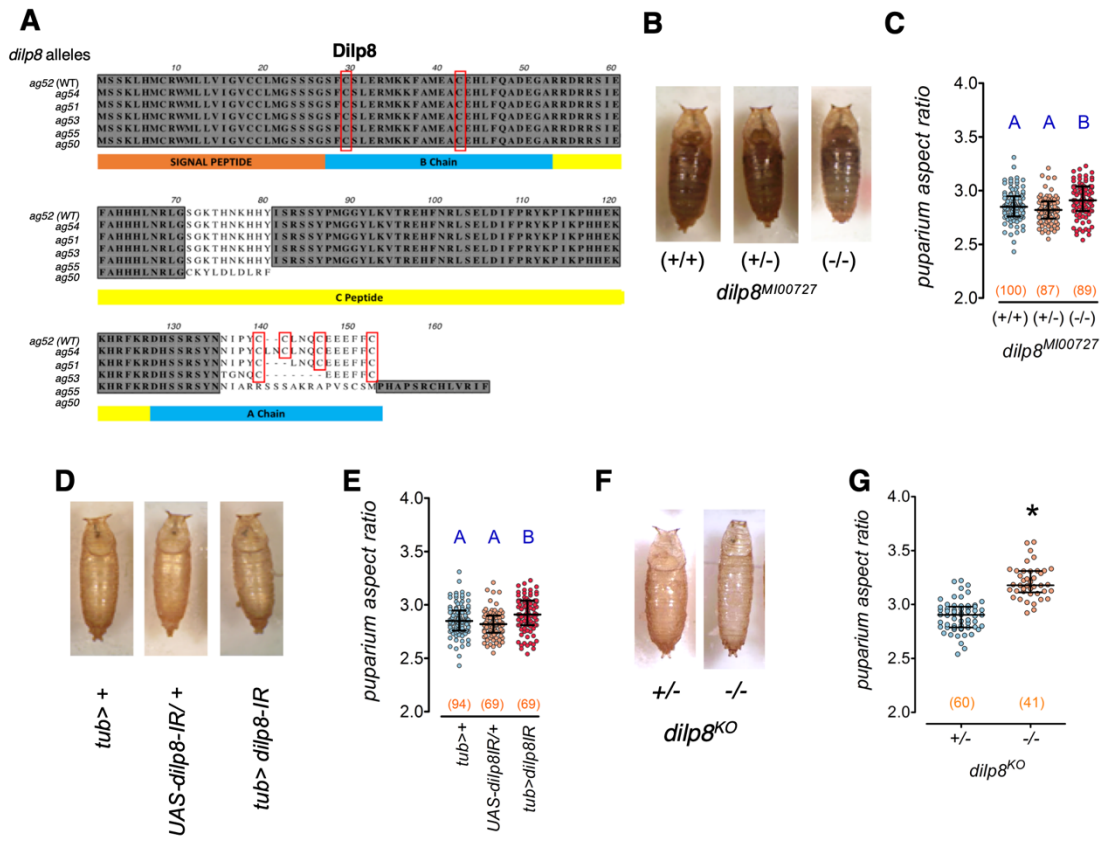

Extended Data Figure 1: CRISPR-Cas9-generated germline *dilp8* mutants and phenotypes of hypomorphs and a knockout.

A. Protein sequence of one wild type *dilp8*^{ag52} and five *dilp8* mutant alleles (*dilp8*$^{ag50-55}$) generated by CRISPR-Cas9 mediated mutagenesis directed to the 3' end that encodes the A-chain with the highly conserved cysteines essential for Dilp8 activity. **B,D,F.** Photos of puparia of **B.** animals carrying the hypomorphic allele *dilp8*^{MI00727} in homozygosis (-/-) or heterozygosis (+/-) [(+/+), WT controls], **D.** of animals ubiquitously-expressing RNAi against *dilp8* (*tub>dilp8-IR*) and controls (*tub> and UAS-dilp8-IR),* and **F.** *dilp8*^{KO} mutants (-/-) and controls (*dilp8*^{KO}/+). **C,E,G.** Dot plots of puparium aspect ratio (AR). Dots, one animal. **B,C.** *dilp8*^{MI00727} mutants and **D,E.** *Tub>dilp8-IR* animals do not show clear alterations in puparium shape nor a strong and consistent change in puparium AR. **F,G.** *dilp8*^{KO} mutants have increased puparium AR. Statistics: **C,E,F.** Horizontal bar, median. Error bars: 25-75% percentiles. **C.** Dunn's test. **D.** Student-Newman-Keuls test. **G.** Student's t-test. Same blue letters, P>0.05. G. * P<0.05. (N) number of animals (red).

Extended Data Figure 2.

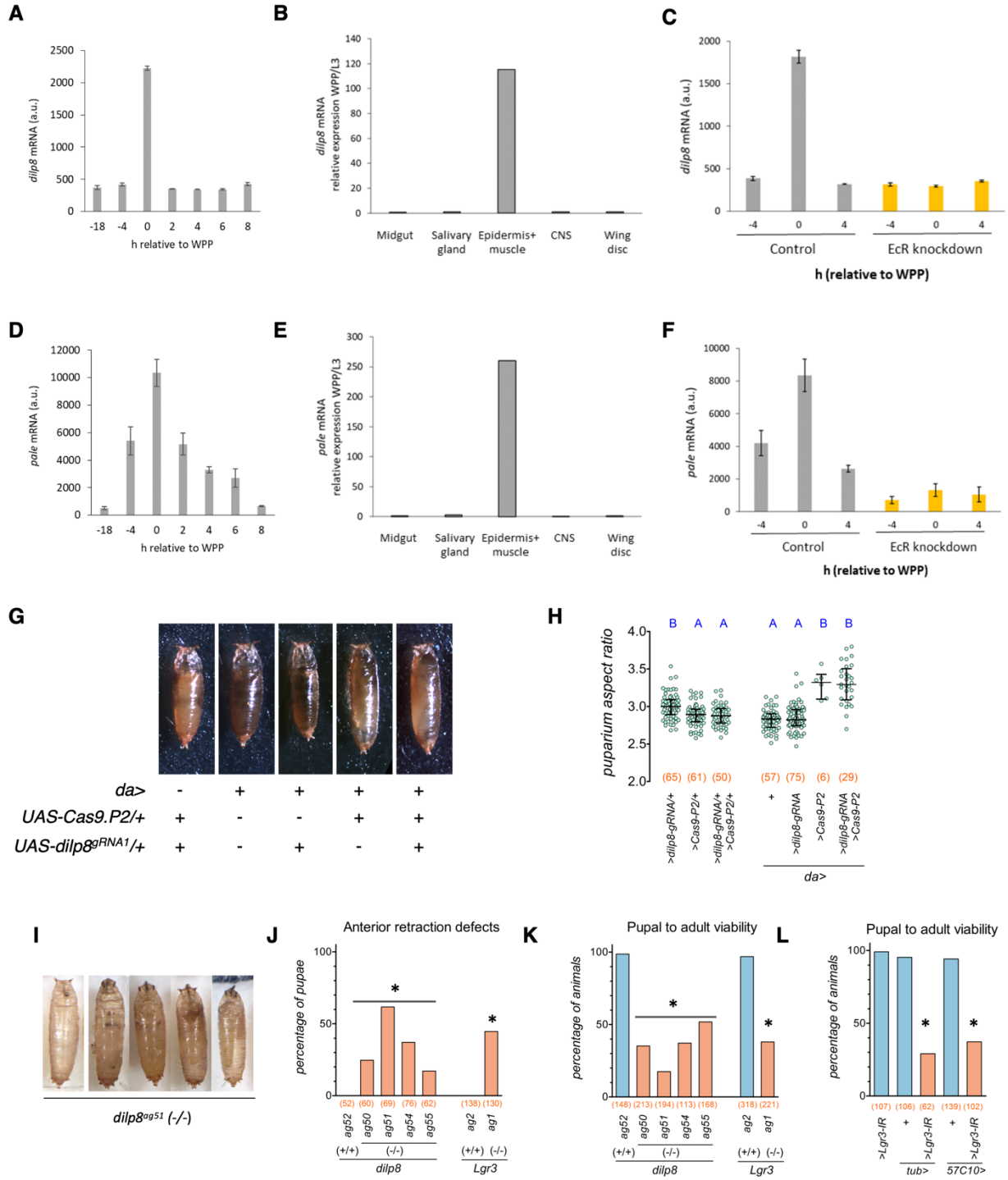

Extended Data Figure 2: *dilp8* and *pale* expression profiles, tissue-specific CRISPR-Cas9 and other phenotypes

A-C. Expression of *dilp8* and **D-F**. *pale* at pupariation [**A,B,D,E,** ref.[55]; **C,F,** ref.[56]]**.please check, it is A,C,D,F from one paper and B,E from another A.** *dilp8* and **D**. *pale* expression peak with different dynamics in white prepupa (WPP T0). **B**. *dilp8* and **D**. *pale*

are upregulated in the WPP-T0 carcass (muscle and epidermal cells). **C,F**. Ecdysone receptor (EcR) knockdown prevents **C**. *dilp8* and **F**. *pale* upregulation at WPP T0. **G,I**. Pictures of animals **G**. ubiquitously-expressing (*da-GAL4, da>*) *UAS-Cas9P2* and/or *UAS-dilp8*^{gRNA1} for targeted somatic mutagenesis of *dilp8* (Cas9 alone affects puparium morphology), and **I**. *dilp8*-mutant puparia displaying increasingly severe anterior retraction defects. **H.** Dot plots of puparium aspect ratio following ubiquitous *Cas9* and/or *dilp8*^{gRNA1}. **J.** Proportion of puparia with defective anterior retraction. **K,L.** Pupal viability is reduced in **K.** animals lacking *dilp8* and *Lgr3* or **L.** following ubiquitous (*tub>*) or panneuronal (*R57C10>*) *Lgr3* knockdown. Statistics: **A,C,D,F.** Average. **A,C,D,F.** Error bars, standard deviation. **H.** Horizontal bar, median. Error bars: 25-75% percentiles. Dunn's test. **J-L.** Binomial tests with Bonferonni corrections. **P*<0.001. (N) number of animals (red).

Extended Data Figure 3.

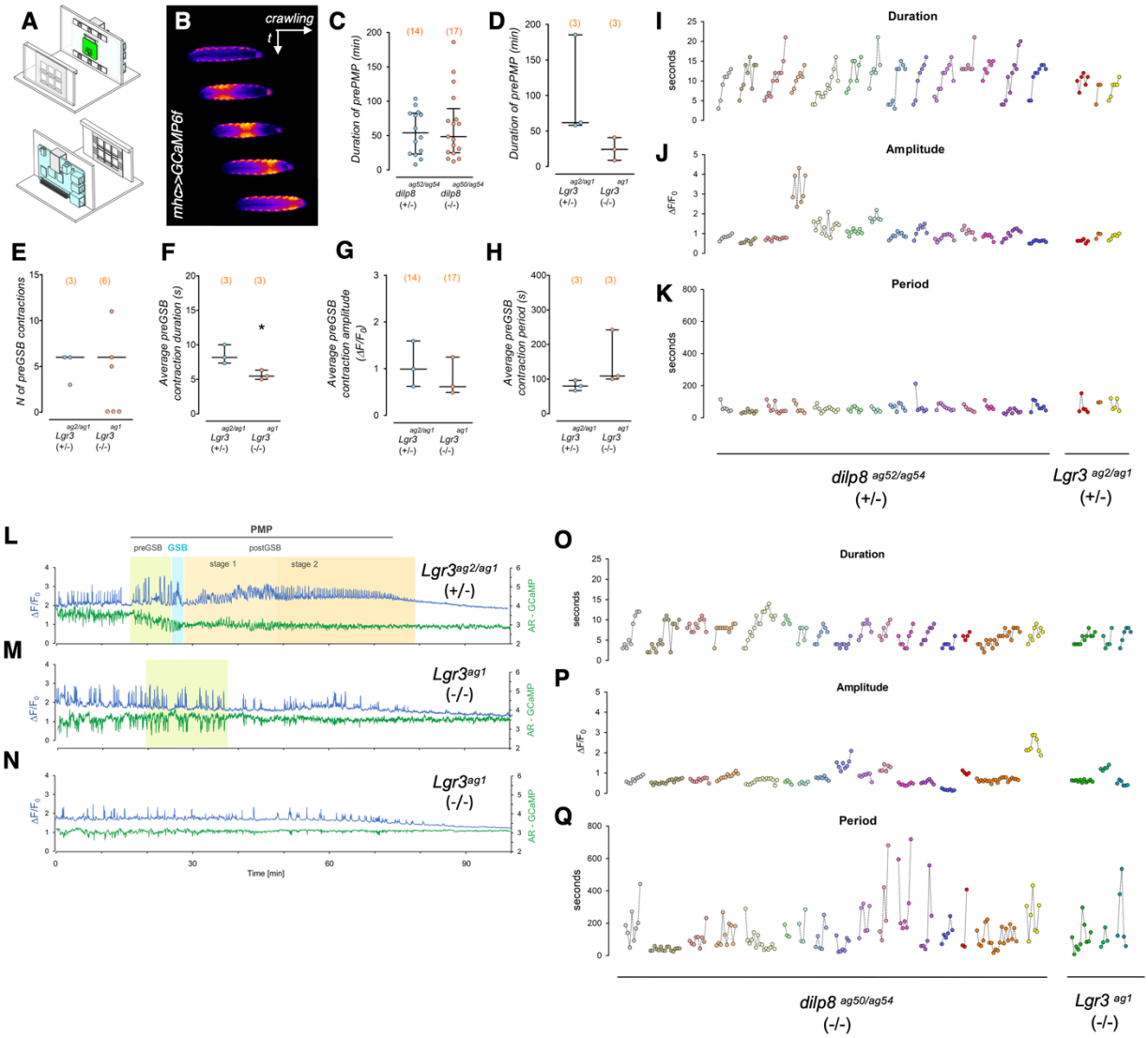

Extended Data Figure 3: Effects of *dilp8* and *Lgr3* on pre-PMP and pre-GSB.

A. Schematics of the pupariation monitoring device. **B.** Time-lapse of a larva expressing the muscle-specific calcium sensor, mhc>>GCaMP, showing peristaltic contractions during larval crawling. **C-H.** Dot plots showing **C,D.** pre-pupariation motor program (pre-PMP) duration in **C.** *dilp8* and **D.** *Lgr3* mutants, and **E.** number (dots: one animal) and average **F.** duration, **G.** amplitude, **H.** period (dots: average per larva) of pre-GSB contractions in *Lgr3* mutants and controls. **I.** Duration, **J.** amplitude, and **K.** period of preGSB contraction in WT animals. Dots connected with a line represent consecutive contractions of one larva. **L-N.** Temporal profile of GCaMP fluctuations (blue) and AR (green) in **L.** WT and **M,N** *Lgr3* mutant animals**. M,N.** *Lgr3* mutants either show pre-GSB-like contractions (**M),** or not (**N**). **O.** Duration, **P.** amplitude, and **Q.** period of pre-GSB contractions in *dilp8* and *Lgr3* mutants.

Statistics: **C-H.** Horizontal bar, median. Error bars: 25-75% percentiles. **C.** Mann-Whitney test. **D-H.** Student's t-test. **C,D,E,G,K.** P=0.86, 0.15, 0.33 (animals without contractions excluded), 0.09, and 0.21, respectively. *P<0.05. (N) number of animals (red).

Extended Data Figure 4.

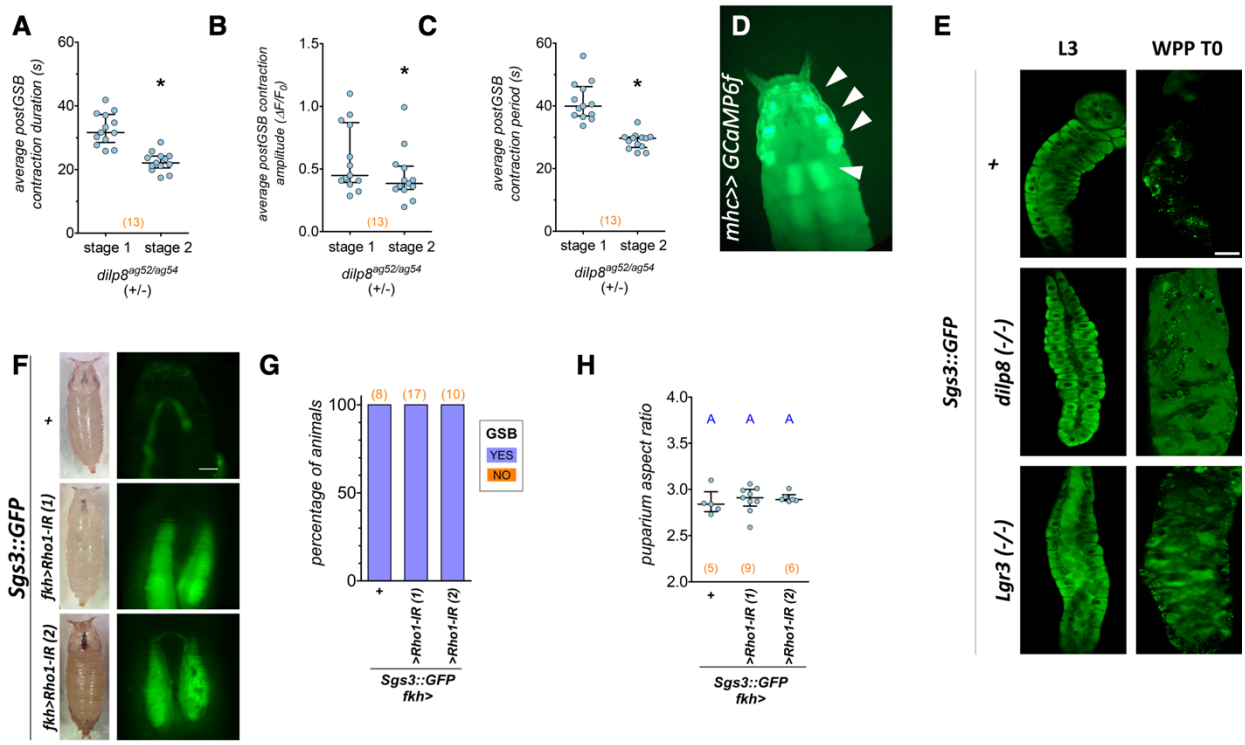

Extended Data Figure 4: Post-GSB stages, operculum formation program, and effects of glue expulsion on puparium morphology and GSB.

A-C,H. Dot plots of **A.** duration, **B.** amplitude, **C.** period (dots: average per larva) of post-GSB contractions according to stages in WT animals, and **H.** puparium aspect ratio (AR) of animals expressing two different RNAi constructs against *Rho1* (*>Rho1-IR(1)* and *>Rho1-IR(2)*) in the salivary gland (using *fkh-GAL4, fkh>*). **D.** Photo of mch>>GCaMP fluorescence in a WT animal during operculum formation stage. **E.** Confocal sections of dissected salivary glands of the depicted genotypes at L3 (wandering) and WPP T0 (pupariation) stage. **F.** Photos of WPP T0 puparia and Sgs3::GFP (green) showing that knockdown of *Rho1* in the salivary gland (*fkh>Rho1-IR*) impedes glue expulsion, but does not **G.** affect GSB (percentage of pupa performing GSB) or **H.** puparium AR. Statistics: **A-C,H.** Horizontal bar, median. Error bars: 25-75% percentiles. **A-C.** Paired Student's t test **G.** Binomial test with Bonferonni corrections. **H.** Dunn's test. Same blue letters, $P>0.05$. **B.** *$P<0.05$. (N) number of animals (red). Scale bar:30 um **E**. 200 um **F**.

Extended Data Figure 5.

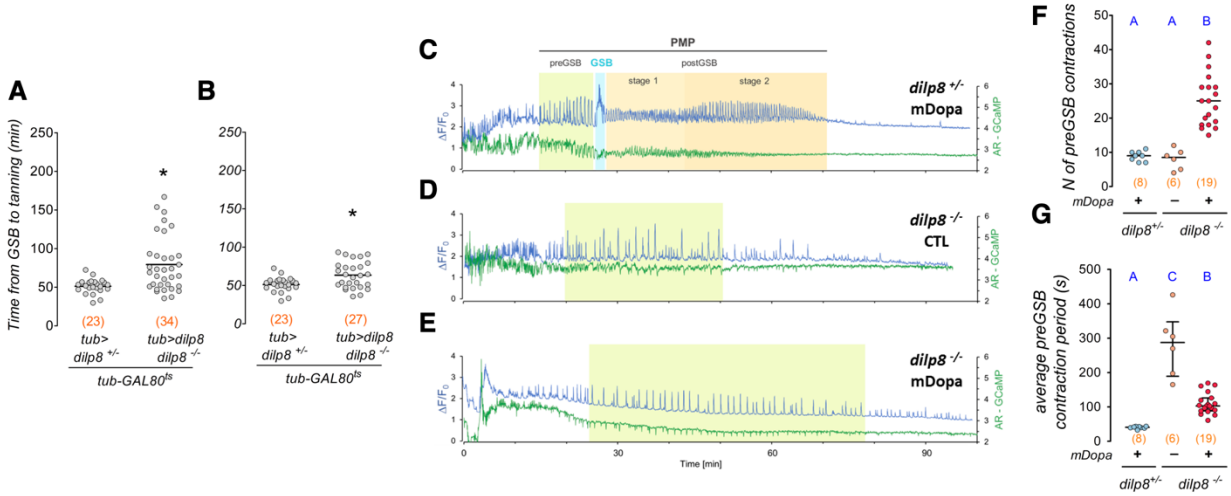

Extended Data Figure 5: Pupariation progression requires coupling of morphogenetic and neuromotor subprograms by the Dilp8-Lgr3 pathway.

A,B,F,G. Dot plots of **A,B.** time from GSB to tanning following removal of animals with **A.** double GSB or **B.** animals with time >100 min, **F.** number and **G.** average period of pre-GSB contractions. **C-E.** mhc>>GCaMP (blue) and aspect ratio (AR-GCaMP, green) fluctuations in **C.** WT and **D,E**. *dilp8* mutants treated (**C,E**) or (**D**) not with α-methyldopa. **A,B.** Post-MIT-expression of *tub>dilp8* delays tanning. **C.** PMP depicting stages. PMP is not overtly altered by α-methyldopa treatment of WT animals. **D.** Non-treated and **E.** α-methyldopa-treated *dilp8* mutants only show pre-GSB-like contractions, never transitioning to GSB. **F,G.** α-methyldopa treatment **F.** increases the number and decreases the average period of pre-GSB contractions in *dilp8* mutants. Statistics: Horizontal bar, **A,B.** average or **F,G.** median. Error bars: 25-75%. **A,B.** Mann-Whitney Rank sum test. **F,G.** Dunn's test. Same blue letters, $P>0.05$. $*P<0.05$. Scale bars, 50 µm.

Extended Data Figure 6.

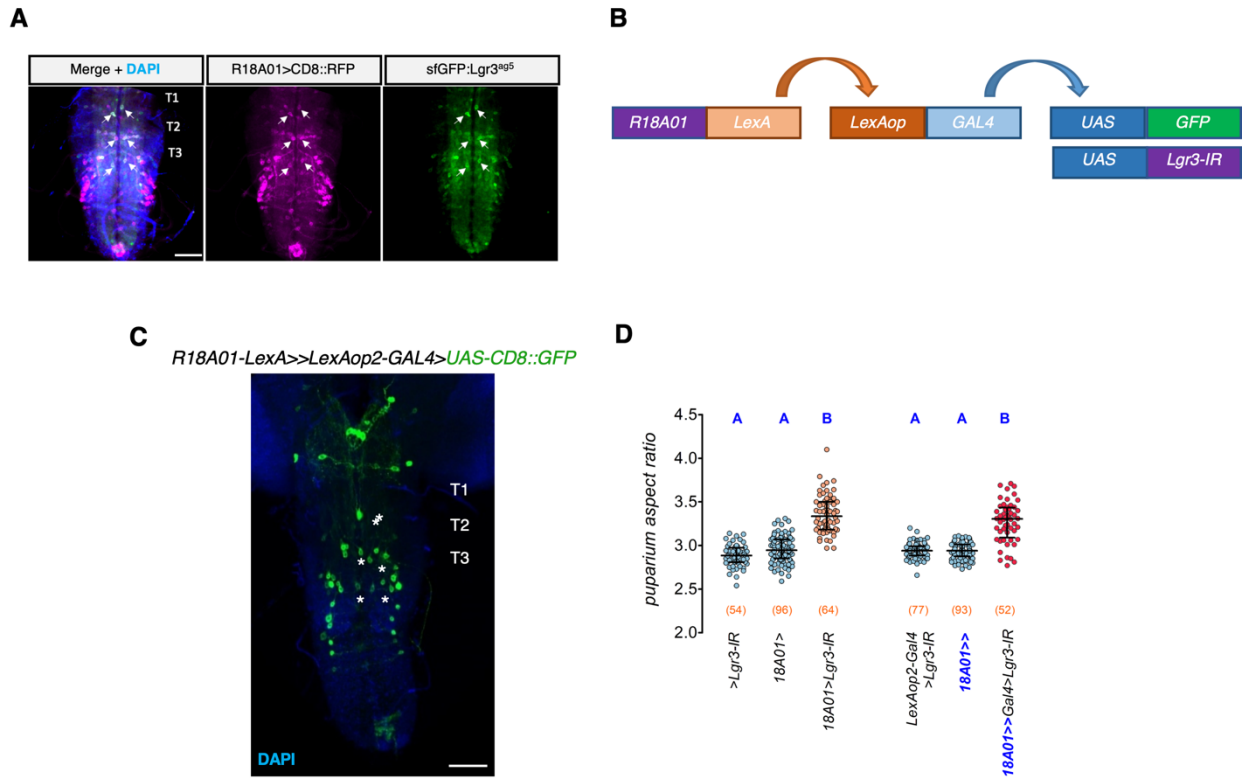

Extended Data Figure 6: *R18A01* expression pattern and validation of *R18A01-LexA* tools.

A,C. Projections of confocal sections of a dissected white prepupa T0 CNS. **A.** Six thoracic (6VNC) interneurons (white arrows) coexpress *R18A01>CD8::RFP* (magenta) and *sfGFP::Lgr3*^{ag5} (anti-GFP, green). DAPI, blue. **B.** Strategy for testing whether or not the *R18A01-LexA (R18A01>>)* line drives expression in the same *Lgr3*-sensitive cells that are important for pupariation behavior control as the *R18A01-GAL4* (*R18A01>*) line. *R18A01>>* drives expression of LexA which drives expression of GAL4 (*LexAop-GAL4*, *13xLexAop2-GAL4v-VP48*), which then drives expression of either *UAS-Lgr3-IR* or *UAS-CD8::GFP*. This is critical to generate a functional intersection, such as the *R18A01∩R48H10* intersectional genetics system. **C.** *R18A01>>CD8::GFP* is expressed in the same 6VNC cells (asterisks) as *R18A01>*. T1-3, thoracic segments. **D.** Dot plots of puparium aspect ratio (AR). *Lgr3* knockdown under the control of *R18A01>* or *R18A01>>* increases puparium AR. Statistics: **D.** Horizontal bar, median. Error bars, 25-75%. Same blue letters, *P*>0.05. Dunn's test. (N) Number of animals (red).

Extended Data Figure 7.

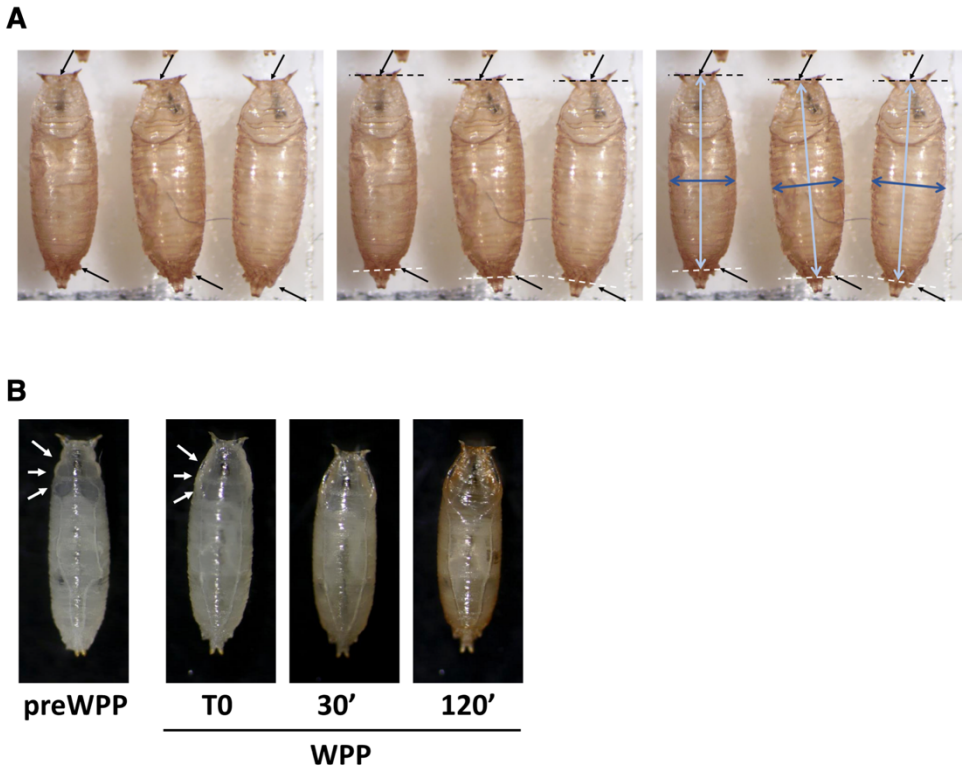

Extended Data Figure 7: Criteria for puparium aspect ratio and pupa staging

A. Measurement of the AR. The black arrows point to the anterior edge and the most anterior anal papillae that were taken as reference to measure the length of the pupa (light blue arrows). A perpendicular line drawn in the widest region of the pupae was used to measure the width. Aspect ratio was calculated as Length/Width. **B.** Morphological features of a white prepupa (WPP = T0). A larva is considered to have reached the WPP stage when the operculum first becomes evident, the most anterior segments flatten in the dorso-ventral direction, and their edges thicken and lose the wiggly appearance (arrows). preWPP = animals that have started pupariation, but have not yet reached the WPP stage. Detectable tanning at WPP occurs ~30 min after T0.